Hydrol. Earth Syst. Sci. Discuss., 8, 9113–9171, 2011
www.hydrol-earth-syst-sci-discuss.net/8/9113/2011/
doi:10.5194/hessd-8-9113-2011

Hydrology and Earth System Sciences Discussions

Improving evapotranspiration in land surface models by using biophysical parameters derived from MSG/SEVIRI satellite

N. Ghilain[1], A. Arboleda[1], G. Sepulcre-Cantò[1,*], O. Batelaan[2,3], J. Ardö[4], and F. Gellens-Meulenberghs[1]

[1]Royal Meteorological Institute of Belgium, Avenue circulaire 3, 1180 Brussels, Belgium
[2]Dept. of Hydrology and Hydraulic Engineering, Vrije Universiteit Brussel, Pleinlaan 2, 1050 Brussels, Belgium
[3]Dept. Earth and Environmental Sciences, Katholieke Universiteit Leuven, Celestijnenlaan 200E, 3001 Heverlee, Belgium
[4]Dept. Physical Geography and Ecosystems Analysis, Lund University, Sölvegatan 12, 223 62 Lund, Sweden
[*]now at: Institute for Environment and Sustainability, Joint Research Center, Ispra, Italy

Received: 29 September 2011 – Accepted: 6 October 2011 – Published: 14 October 2011

Correspondence to: N. Ghilain (nicolas.ghilain@meteo.be)

Published by Copernicus Publications on behalf of the European Geosciences Union.

Abstract

Vegetation parameters derived from the geostationary satellite MSG/SEVIRI have been distributed at a daily frequency since 2007 over Europe, Africa and part of South America, through the LSA-SAF facility. We propose here a method to handle two new remote sensing products from LSA-SAF, leaf area index and Fractional Vegetation Cover, noted LAI and FVC respectively, for land surface models at MSG/SEVIRI scale. The developed method relies on an ordinary least-square technique and a land cover map to estimate LAI for each model plant functional types of the model spatial unit. The method is conceived to be applicable for near-real time applications at continental scale. Compared to monthly vegetation parameters from a vegetation database commonly used in numerical weather predictions (ECOCLIMAP-I), the new remote sensing products allows a better monitoring of the spatial and temporal variability of the vegetation, including inter-annual signals, and a decreased uncertainty on LAI to be input into land surface models. We assess the impact of using LSA-SAF vegetation parameters compared to ECOCLIMAP-I in the land surface model H-TESSEL at MSG/SEVIRI scale. Comparison with in-situ observations in Europe and Africa shows that the results on evapotranspiration are mostly improved, and especially in semi-arid climates. At last, the use of LSA-SAF and ECOCLIMAP-I is compared with simulations over a North-South Transect in Western Africa using LSA-SAF radiation forcing derived from remote sensing, and differences are highlighted.

1 Introduction

In the past decades, an increasing number of models were developed to monitor evapotranspiration at different scales using remote sensing measurements. Simple empirical or statistical methods to fully detailed physical models have been developed, using a wealth of information provided by various satellites (e.g. Courault et al., 2005; Kalma

HESSD
8, 9113–9171, 2011

et al., 2008; Li et al., 2009). In all methods, vegetation has been recognized to be a cornerstone of the evapotranspiration process, since plants are the main medium for exchange of water between the soil and the atmosphere. In particular, land surface models are widely used for meteorological and climate studies. They are based on a conceptual and semi-empirical description of, respectively, the physical and physiological processes of heat and water exchanges between soil, plants and atmosphere media. Information usually needed for land surface models is (1) the exact coverage of Plant Functional Types (PFT), information given by a land cover map, (2) the state of the vegetation development, mostly given by the variable Leaf Area Index (LAI). While most of those models require explicit external information on the vegetation status (e.g. Balsamo et al., 2009; Noilhan and Planton, 1989), a new generation of models considers it as a new model variable (e.g. Jarlan et al., 2008; Gibelin et al., 2006; Blyth et al., 2006). But, for both classes, information on vegetation status is highly important. For the first class of models, it is a necessary information to provide. For the second one, it is recommended for updating the model forecasts (e.g. Jarlan et al., 2008; Albergel et al., 2010), or at least evaluate their output (e.g. Brut et al., 2009). Past studies have used variety of land surface models or crop growth models and different vegetation products issued from remote sensing (e.g. Dorigo et al., 2006). By this way, the use of remote sensing vegetation indices has revealed an improvement of the mean quality of surface variables forecasting.

Along with the ever growing length of time series available from remote sensing have come different exploitations of that remote sensing information. Early usage of the remote sensing vegetation indices in Soil-Vegetation-Atmosphere Transfer (SVAT) models focused on a mean vegetation status by plant type throughout a year. New available long time series and reprocessing capabilities gave rise to vegetation databases, that include a mean monthly or weekly evolution of vegetation parameters, PFT and geographically dependent (e.g. ECOCLIMAP). Those two approaches have been widely used for operational purposes (e.g. van den Hurk et al., 2000, 2003) for practical reasons: easy to handle, not dependent on necessary incoming information from an

HESSD
8, 9113–9171, 2011

external source, and hence on timeliness. However, the direct use of remote sensing time series is an important step towards a closer monitoring of the land surface, because it captures better both spatial and temporal variations, including intra-species and inter-annual variability.

Previous efforts have been carried out mainly using time series from polar orbiters (e.g. Albergel et al., 2010; Rodell et al., 2004). However, most of those studies focus on assimilation in a reanalysis mode, and cannot be used for a near-real time monitoring of the surface turbulent fluxes. Recently, the EUMETSAT Land Surface Analysis Satellite Application Facility (LSA-SAF) developed a coordinated service in the area of remote sensing of the land surface and proposes products based on the geosynchronous MSG satellites (http://landsaf.meteo.pt) (Trigo et al., 2011). Among these products, remotely sensed biophysical parameter products, i.e. leaf area index, LSA-SAF LAI, and fractional vegetation cover, LSA-SAF FVC, are delivered daily at MSG/SEVIRI resolution (LSA-SAF PUM VEGA, 2008), and are available since 2007. This study focuses on the applicability and gain of using biophysical parameters issued from geostationary satellites, compared to monthly varying databases, for land surface modelling applications, including near-real time monitoring, at the meso-scale resolution of MSG/SEVIRI.

In the remaining of this paper, we describe the method we developed to use LSA-SAF biophysical parameters in a land surface model at the same resolution, a set of validation results over Europe and Africa, as well as an example of application over West Africa. In Sect. 2, we describe the remote sensing derived variables and products used. In Sect. 3, we give a short description of the land surface model, as well as its field of application and forcings. In Sect. 4, we develop a robust methodology to use the LSA-SAF LAI and FVC in the land surface models, in view of operational implementation. Post-processed LSA-SAF vegetation products are then compared to a vegetation database intended for land surface models (ECOCLIMAP-I) in Sect. 5. In Sect. 6, the impact on evapotranspiration of using LSA-SAF vegetation products following our methodology is assessed by comparison against in-situ observations in Europe and Africa. As well, the impact on evapotranspiration monitoring over western

HESSD
8, 9113–9171, 2011

Africa is illustrated, compared to the use of ECOCLIMAP-I. The use of land covers for long term near-real monitoring of evapotranspiration using MSG satellites is discussed in Sect. 7. At last, conclusions from this work are outlined.

2 Remote sensing platforms for large-scale observation of vegetation and use in land surface models

At large scale, only remote sensing provides a reliable monitoring of vegetation. Different remote sensing platforms now provide: hyperspectral, thermal remote sensing from polar orbiters (MODIS, MERIS, SPOT/VEGETATION) or geosynchronous satellites (MSG, GOES). Vegetation indices are retrieved through the inversion or ratios of spectral data provided by such satellites. In the first attempts, NDVI and SAVI indices have been widely used to characterize the vegetation properties at the surface. Advances in inversion techniques are now used to infer more geometrical and physical properties of the vegetation, including the leaf area index, LAI (e.g. Baret et al., 2007), the fraction covered by the vegetation, Fveg, and the fraction of absorbed radiation by vegetation through photosynthesis, FAPAR (e.g. Gobron et al., 2006). Remote sensing observations provide therefore the tools to build essential information for land surface modelling: land cover maps and biophysical parameters, useful to quantify the turbulent exchanges between the vegetation and the atmosphere.

2.1 Land covers

A land cover map is required for most land surface models, as it allows the model to select biophysical parameters according to the plant functional type. The land cover map is a very useful property derived from remote sensing at global scale, and is envisaged as fixed or regularly updated. In numerical weather forecast models (e.g. ALADIN International Team, 1997), ECOCLIMAP-I (Masson et al., 2003; Champeaux et al., 2005) is often used. An enhanced land cover, ECOCLIMAP-II, has been developed (Faroux

HESSD
8, 9113–9171, 2011

et al., 2007; Kaptué Tchuente et al., 2010), and will probably soon be publicly available. Other land cover maps used in land surface modelling applications, e.g. IGBP (Loveland et al., 2000), GLC2000 (Bartholomé and Belward, 2005), GlobCover (Bicheron et al., 2006) and MODIS (land cover type yearly L3 Global 500 m) MCD12Q1 v005, are freely available. The spatial resolution of those land covers range from 300 m to 1 km. For a thorough comparison of those land cover regarding the remote sensing data used and methodology, the reader can refer to Kaptué Tchuente et al. (2010). ECOCLIMAP-I is adopted in the present study, but GlobCover V2.2 (Bicheron et al., 2008) and MODIS MCD12Q1 v005 are used as well for assessing the impact of land cover differences.

2.2 Biophysical parameters

Three main biophysical parameters are required for a land surface model simulation. First, LAI is the commonly adopted biophysical parameter for land surface models. Physically, LAI allows the determination of the number of stomata available for plant transpiration and is usually necessary to scale internal model parameters from a single leaf, for which model parameters are better known and modulate according to the PFT, to a coarser resolution. In addition to LAI, the fraction of the surface covered by green vegetation, Fveg, is also important, because it allows computing an energy balance separately on vegetation covers and soil in a dual way (e.g. Anderson et al., 2007). Fveg is usually linked to LAI through an exponential relation, following Beer law of light extinction through canopy (e.g. Kaptué Tchuente et al., 2010). That latter formulation takes into account geometrical properties of different PFTs (Chen et al., 2005), like the leaves inclination or the volumetric configuration. At last, the roughness lengths for momentum and for heat, $z_{0,m}$ and $z_{0,h}$, are structural parameters used in land surface models. They depend on the vegetation (Brutsaert, 1982), that acts as a roughness element to turbulent transfers from the surface to the atmosphere. As roughness lengths are hardly measured globally, several studies propose formulations allowing their computation from LAI (e.g. Verhoef et al., 1997).

HESSD
8, 9113–9171, 2011

First land surface modeling applications made use of synthetic look-up tables (e.g. van den Hurk et al., 2000). To each PFT was associated a prescribed set of model biophysical parameters, that were more internal parameters than observation-based. With the advances in quantitative remote sensing of the land surface, more and more biophysical parameters were made available, and especially LAI, which supports deriving the other parameters as well. Now, a large range of remotely sensed LAI data is available, at different spatial and temporal scales.

Two different approaches for using those remote sensing derived LAI data have been developed: (1) defining a synthetic database, or an evoluated look-up table, that could be used in models (e.g., Masson et al., 2003; Lawrence and Chase, 2007), or (2) using it directly in the models. While the second approach has been used in several research studies, it is barely used in operational models. Both approaches are compared here using (1) ECOCLIMAP-I database, and (2) LSA-SAF biophysical parameters.

ECOCLIMAP-I, additionally to the land cover map at 1 km resolution, is also a synthetic global vegetation database that provides a vegetation parameterization for use in SVAT models. It is widely used by numerical weather prediction models in European countries, and also used for inter-comparison of land surface models in Western Africa (Boone et al., 2009; Grippa et al., 2011). Each PFT is associated to a 10 days or monthly varying set of biophysical parameters, averaged spatially over all the grid cells occupied by the concerned ecosystem. Decomposition of the ecosystems into plant functional types is also determined. Simple formulas are used to derive Fveg from NDVI, LAI, albedo and emissivity from Fveg, and roughness lengths, $z_{0,m}$ and $z_{0,h}$, from LAI.

The utility of LSA-SAF LAI and FVC products (García-Haro et al., 2005) is investigated in the present study. Those biophysical parameters are derived from MSG/SEVIRI and use a two components Spectral Mixture Analysis method (García-Haro et al., 2005b; Verger et al., 2009). LSA-SAF produces daily LAI and FVC, based on the past 5-days estimations, at the sensor spatial resolution. Retrieval uncertainty, as well as a quality flag indicating the quality and reason for possible no production

HESSD
8, 9113–9171, 2011

(e.g. snow, traces of snow, traces of inland water) is also provided (LSA-SAF PUM VEGA, 2008). LSA-SAF products represent an interesting alternative to SPOT-VGT or MODIS for meso-scale applications, in respect to its relatively high generation frequency and its relative time stability compared to MODIS LAI product. LSA-SAF LAI and FVC have been produced routinely since August 2005, with successive algorithm (VEGA) improvements, related to methodology (VEGA v2.0, September 2006), input data quality (December 2006), and post-processing (VEGA v2.1, May 2008).

For long-term monitoring of ET, it is necessary to capture the inter-annual variability of the signal, which can be caused, for example, by a different date of bud-break for deciduous forests, harvest timing shifts (Cooley et al., 2005), rain occurence in semi-arid areas, where the vegetation growth is driven by the hydrological regime, or else by land re-affection or fires. For the short term monitoring, at a daily time scale, poor time sampling of the vegetation phenology can have negative impact on ET, especially during the rapid development stage of the canopy (e.g. Sepulcre-Cantó et al., 2011). Moreover, even if the classification in ecosystems of ECOCLIMAP-I is quite fine, the assumption of equal properties across different spatial scales for one ecosystem seems to be a large simplification of the problem.

3 Model and forcing

3.1 The land surface model

The host land surface model for this study is based on H-TESSEL, the ECMWF land surface model (Beljaars and Viterbo, 1994; Viterbo and Beljaars, 1995; van den Hurk et al., 2000; Balsamo et al., 2009). It follows a bulk resistance formulation for the estimation of the surface turbulent fluxes, with two resistances modulating the variation of the sensible and latent heat fluxes. The aerodynamical resistance accounts for the turbulence generated by air temperature or wind gradient, while the stomatal resistance includes the influence of vapor pressure deficit, fraction of absorbed energy and soil

HESSD
8, 9113–9171, 2011

water availability on the opening of the leaves stomata via a simple parameterization (van den Hurk et al., 2000). In addition, vertical distribution of moisture and temperature in the soil is modeled as a solution to diffusion equations. The modified formulation for the runoff and soil coefficients (Balsamo et al., 2009) is adopted, taking into account differences in soil properties and topography effects. As well, direct evaporation from interception is modelled. The needed forcing of this model consists in short and long-wave radiation reaching the land surface, surface albedo, wind speed, air temperature and air humidity at a blending height. In this model, the spatial unit for the energy balance assessment is divided into different tiles that are associated to plant functional types (Bonan et al., 2002), a common feature of most land surface models. The estimation of the surface fluxes is performed for each PFT before averaging over the spatial unit. The formulation uses parameters describing the vegetation state for each PFT separately. The different parameters related to the vegetation needed by the model are LAI, Fveg, $z_{0,m}$, $z_{0,h}$, a model parameter specific to each vegetation type, i.e. minimum stomatal resistance, and the vertical distribution of the roots in the soil. The PFT classes have been changed from the original formulation of H-TESSEL to match the classification of ECOCLIMAP-I (Ghilain et al., 2011) and the model parameters have been calibrated.

3.2 Field of application, resolution and forcing

The adapted H-TESSEL model can be used at different spatial scales, from a single point simulation using local measurements as input up to coarse grids used by global circulation models. In this paper, the model is mostly used at meso-scale, since we are interested in assessing the utility of the LSA-SAF biophysical parameters for land surface models. We therefore work with the MSG/SEVIRI grid. The basic spatial unit of the model corresponds to the MSG/SEVIRI pixel, i.e. 3 km spatial resolution at the sub-satellite point. The MSG/SEVIRI field of view covers Europe, Africa and part of South America. From the total area monitored by MSG/SEVIRI, four geographical areas (Europe, North and South Africa, South America) have been defined in LSA-SAF. In this

HESSD
8, 9113–9171, 2011

paper, we will focus on Europe (Euro) and Africa (NAfr and SAfr). Besides the biophysical parameters, LSA-SAF produces in near-real time the radiative terms used in land surface models. The radiative terms used here are the downward surface short-wave and long-wave fluxes (Geiger et al., 2008a; Ineichen et al., 2009), LSA-SAF DSSF and DSLF, and the surface albedo (Geiger et al., 2008b; Carrer et al., 2010), LSA-SAF ALBEDO. LSA-SAF DSSF and DSLF are produced half-hourly, while surface albedo is produced daily. Meteorological forcing is provided by a Global Circulation Model, the ERA-Interim re-analyses (Simmons et al., 2006). The spatial resolution available is 0.5°and temporal sampling is 3 h. Meteorological forcing is linearly interpolated in time to half-hourly values. Tri-hourly precipitation rates are distributed equally for each 30 min steps. If radiative forcing is missing, ERA-Interim is used to fill the gaps. Complementary information on vegetation is needed: a land cover map and biophysical parameters. Since each pixel can be composed of different PFTs, biophysical parameters must be known for each PFT inside the pixel, as well as the exact percentage that the PFTs occupy. The land surface model outputs an evapotranspiration estimate for each 30 min time step. In the next section, we describe the way we handle ECOCLIMAP-I database and the proposed scheme for using LSA-SAF biophysical parameters in the land surface model.

4 ECOCLIMAP-I and LSA-SAF LAI: methodological development for use in the land surface model

4.1 Practical use of ECOCLIMAP-I

ECOCLIMAP-I consists of a land cover of ecosystems at 1 km resolution, and a set of monthly biophysical parameters, i.e. LAI, Fveg, $z_{0,\mathrm{m}}$, for each ecosystem. As well, the decomposition of mixed ecosystems into PFTs (Table 1) is provided. ECOCLIMAP-I is used as in Ghilain et al. (2011). In order to use it for the vegetation parameterization of our host model, we decompose the ecosystems into PFTs, and project the land cover

HESSD
8, 9113–9171, 2011

obtained from the original 1 km resolution onto the coarser grid defined by the model. We consider as appropriate to limit the number of PFTs to five at maximum. The land cover obtained gives the 5 dominant PFTs and their contribution to a MSG/SEVIRI pixel. But, since one PFT can result from the combination of several ecosystems, LAI for each PFT is computed as the weighted mean contribution of the involved ecoystems LAI. Monthly LAI maps at MSG/SEVIRI resolution are then created.

4.2 Method for using LSA-SAF LAI and FVC in the land surface model: development

LSA-SAF LAI and FVC images are provided every day at the MSG/SEVIRI spatial scale, i.e. 3.1 km at the sub-satellite point, over the whole field of view. At that scale, landscapes can be very heterogeneous, especially over Europe, and one pixel can represent a mixed signal of different ecosystems or PFTs. This information cannot be used straightforward in SVAT-type models, because of the need to get (1) information on each PFT of the pixel to compute surface fluxes, (2) continuous time series and (3) stable and consistent time series. It is therefore necessary to implement a procedure able to retrieve LAI at sub-pixel or PFT level, and to cope with continuity and stability issues. A two-steps procedure, named P1 and P2 hereafter, is implemented to, first, provide LSA-SAF LAI maps consistent with previous time steps, and then, to compute vegetation parameters for each PFT of the considered pixel.

For each given pixel, P1 consists of building continuous and consistent LAI time series as close as possible to the actual LSA-SAF LAI product, LAI_{SAF}. The procedure described by Gu et al. (2006) for the MODIS LAI over Canada has been adopted. A schematic view of the process is shown in Fig. 1. First, an annual LAI climatology is built pixelwise using daily LSA-SAF LAI images from 2007 to 2010. The climatological year is divided in periods of 10 days. For each 10 days period, a mean LAI, LAI_c, is calculated pixelwise, along with an error bar, σ_c, corresponding to the standard variation

HESSD
8, 9113–9171, 2011

of the LSA-SAF LAI sample used.

$$LAI_c = \frac{1}{N} \cdot \sum_{year\ =\ 2007,2010} \sum_{i=1,10} LAI_{SAF,i,year} \quad (1)$$

Even if snow cover is flagged, some spurious data, occuring especially during the 2007–2008 winter in northern latitudes and over coniferous forests, still persist. Similar problems have been encountered by Jiang et al. (2010) with NOAA satellite. In May 2008, LSA-SAF changed the algorithm to VEGA v2.1 to screen those data by applying a post-processing on the problematic areas. However, we want here to take advantage of longer time series available. The spurious data are filtered out using a threshold. Winter LAI higher than 85 % of the mean summer value are filtered out. The extent of the winter is based on the collection of the spurious data: it is longer for Northern european countries (e.g. Sweden, Finland) and shorter for the european mid-latitude countries (e.g. Germany, France). A linear interpolation is applied on both LAI values and standard deviations to fill the gaps in the climatological series, responding to the demand of operational models (Jiang et al., 2010). Finally, for each actual LSA-SAF LAI to be used, an optimal interpolation scheme (Gu et al., 2006) is applied. As LSA-SAF LAI time series are more stable in time than the MODIS LAI (LSA-SAF PUM VEGA, 2008), a less conservative choice can be applied in our study. Therefore, in our scheme, errors on the climatology, σ_c, can be multiplied by 2.5 and are noted $\tilde{\sigma}_c$. In consequence, the weight of the climatology is decreased to better follow the daily remote sensing product. The result is a LAI for each pixel (LAI_a), corrected using a background information. In that way, most dubious data are removed, the time series are smoother and gaps are filled.

$$LAI_a = \frac{\tilde{\sigma_c}^2}{\sigma_{SAF}^2 + \tilde{\sigma_c}^2} \cdot LAI_{SAF} + \frac{\sigma_{SAF}^2}{\sigma_{SAF}^2 + \tilde{\sigma_c}^2} \cdot LAI_c \quad (2)$$

HESSD
8, 9113–9171, 2011

As in (Gu et al., 2006), when

$$|LAI_{SAF} - LAI_c| > 2 \cdot \sqrt{\sigma_{SAF}^2 + \tilde{\sigma}_c^{\,2}} \quad (3)$$

LAI_{SAF} is said to be unusable, and full weight is set on LAI_c:

$$LAI_a = LAI_c \quad (4)$$

We illustrate the process on one specific LAI time series over Wetzstein, a forested site in Europe (Fig. 2). The MSG/SEVIRI pixel is mainly composed of coniferous forest. LSA-SAF LAI (red points) presents unrealistic high values in the 2007–2008 winter. During the next winters, most of those unrealistic estimates have been screened out in the product, but there still remain some. The LAI climatology (black points) follows the trend given by LSA-SAF LAI, with very high values in winter. Using the filter, we remove all the spurious data, and a linear interpolation is applied. After correction, the optimal interpolation procedure is applied to produce the LAI analysed.

P2 consists basically of an ordinary least-square algorithm (OLS), based on two assumptions: (1) the percentage of each PFT in one pixel represents exactly the real cover of the land surface, (2) the vegetation parameters, e.g. LAI, in close neighbourhood are assumed to be homogeneous. This hypothesis is reasonable if we consider that, in a close neighbourhood to be defined, usually a region of 9 or 25 MSG/SEVIRI pixels (3×3, 5×5), meteorological and climatic conditions are similar, and one can assume the growth of the natural vegetation will be the same for one specific plant type. For human-forced vegetation, like for crops, the assumption can still hold if we assume that agricultural practices are homogeneous in the region of interest, which is often the case for large areas.

With those assumptions, the problem is put into equations, considering a neighbourhood of M pixels.

HESSD
8, 9113–9171, 2011

Let **M** be the linear model matrix, representing the proportion $f_{i,j}$ for each pixel i of determined PFT j.

$$\mathbf{M} = \begin{pmatrix} f_{1,1} & \cdots & f_{1,N} \\ \vdots & \ddots & \vdots \\ f_{M,1} & \cdots & f_{M,N} \end{pmatrix} \quad (5)$$

$\boldsymbol{Y}$ is the observation vector, which contains the LSASAF LAI_i estimates for the M considered pixels.

$$\boldsymbol{Y} = \begin{pmatrix} \mathrm{LSASAF} - \mathrm{LAI}_1 \\ \vdots \\ \mathrm{LSASAF} - \mathrm{LAI}_M \end{pmatrix} \quad (6)$$

Now, let $\boldsymbol{X}$ be the solution vector containing the averaged values V_i over the domain for each involved ecosystem.

$$\boldsymbol{X} = \begin{pmatrix} V_1 \\ \vdots \\ V_N \end{pmatrix} \quad (7)$$

Therefore, the problem has the following simple linear form (Eq. 8).

$$\mathbf{M} \cdot \boldsymbol{X} = \boldsymbol{Y} \quad (8)$$

Taking into account the retrieval uncertainty of the LSA-SAF LAI and assuming it corresponds to the standard deviation of a normal error distribution, we scale the matrix **M** and the observation vector $\boldsymbol{Y}$ by weighting factors, σ_M. A matrix **W** containing the weights is formed (Eq. 9), and new matrix $\mathbf{M}_\mathrm{w}$ (Eq. 10) and vectors $\boldsymbol{Y}_\mathrm{w}$ (Eq. 11) are

HESSD
8, 9113–9171, 2011

defined. We get to solve Eq. (12).

$$\mathbf{W} = \begin{pmatrix} 1/\sigma_1 & 0 & \cdots & 0 \\ 0 & \ddots & \ddots & \vdots \\ \vdots & \ddots & \ddots & 0 \\ 0 & \cdots & 0 & 1/\sigma_M \end{pmatrix} \tag{9}$$

$$\mathbf{M}_\mathrm{w} = \mathbf{W} \cdot \mathbf{M} \tag{10}$$

$$\boldsymbol{Y}_\mathrm{w} = \mathbf{W} \cdot \boldsymbol{Y} \tag{11}$$

$$\mathbf{M}_\mathrm{w} \cdot \boldsymbol{X} = \boldsymbol{Y}_\mathrm{w} \tag{12}$$

Solving the linear set of equation using a least square method, we obtain the LAI for each PFT. The solution in the least square sense using the L2-norm is given by Eq. (13).

$$\boldsymbol{X} = (\mathbf{M}_\mathrm{w}^\mathbf{T} \cdot \mathbf{M}_\mathrm{w})^{-1} \cdot \mathbf{M}_\mathrm{w}^T \cdot \boldsymbol{Y}_\mathrm{w} \tag{13}$$

whereby $\mathbf{M}_\mathrm{w}^T$ is the transpose of $\mathbf{M}_\mathrm{w}$.

To fasten the numerical computation of the solution, as well as to avoid problems often occurring when inverting large sparse matrices, we reduce the matrix $\mathbf{M}_\mathrm{w}$ to its irreducible dimensions, corresponding to the number of pixels times the number of PFTs occupying the size-defined neighbourhood. If the matrix is non-invertible a singular value decomposition algorithm is applied. Repeating the operation by moving the size-defined neighbourhood by one pixel at a time, we obtain a smoothed spatial average estimate of LAI for each PFT.

We should especially care about the correct handling of remote sensing derived LAI in the land surface model. In two examples (Oleson and Bonan, 2000; van den Hurk et al., 2003), land surface models are feeded with remote sensing LAI. Fveg is constant, and LAI varies. In other studies, LAI is constant, while Fveg varies (Jiang

HESSD
8, 9113–9171, 2011

et al., 2010; Miller et al., 2006). In most of those studies, stress is put on not using both simultaneously varying, as they are derived from the same signal, and would be either double counted or vanishing. Both studies from the first stream mention that the remotely sensed LAI is different from the LAI needed by the model (also reported in Ge (2009)): the model needs the LAI of the vegetated part, LAI_v while remote sensing provides LAI for the total area, LAI_{RS}. Therefore, if an area is composed of a fraction X of vegetation and $1-X$ fraction of bare soil, the LAI needed by the model should be:

$$LAI_v = \frac{1}{X} \cdot LAI_{RS} \quad (14)$$

Following those practical advises, we have generated a map to prescribe the fixed fraction of each pixel assigned to be bare soil, this to avoid double effect of using simultaneously fully correlated daily varying FVC and LAI. The percentage of bare soil in a given pixel is determined by 1-min(FVC) over 2007 and 2008. Assuming that the bare soil fraction has a zero LAI, consistent handling of LAI for the land surface model is ensured.

Roughness lengths needed by the model, i.e. $z_{0,m}$ and $z_{0,h}$, are computed from the derived LAI by PFT, as in ECOCLIMAP-I (Eqs. 15 and 16).

$$z_{0,m} = 0.13.h_{veg} \quad (15)$$

$$z_{0,h} = 0.1.z_{0,m} \quad (16)$$

h_{veg} is an effective vegetation mean height, function of LAI (Table 2).

4.3 Analysis and post-processing of derived LSA-SAF LAI at PFT level

The OLS method described above is lead to the exact solution if two assumptions are verified. However, as both assumptions are a simplification of the real world, we need to assess how realistic they are. The land cover map is supposed to represent the true distribution of PFTs. However, it is well known that discrepancies are observed

HESSD
8, 9113–9171, 2011

between different land covers (e.g. Jung et al., 2006). The choice of ECOCLIMAP-I was straightforward as it was already implemented in operational setup (Ghilain et al., 2011). Other land covers derived from higher spatial resolution data could be used: MODIS (MCD12Q1), available at 500 m resolution and updated yearly, and GlobCover, available at 300 m resolution.

As an example of the mentioned differences, two examples over eddy covariance measurement sites (Tojal in Portugal (Pereira et al., 2007) and Hesse in France (Granier et al., 2000)), with the area of the MSG/SEVIRI pixels over Europe, have been extracted from ECOCLIMAP-I, MCD12Q1 (2007) and GlobCover v2.2, and the proportions of PFTs compared together in Fig. 3.

For a selection of 120 locations chosen randomly over the Euro window (Fig. 4), we derived LAI by PFT using each of the three land covers for 2007. For each PFT in each selected pixel, we computed the difference in PFT percentage (rescaled to the vegetated fraction of the pixel). Time correlation and root-mean square difference (RMS) between the LAI series obtained from the 3 land covers are estimated, by PFT and by pixel. Figure 5 shows the relation between the mean PFT percentage obtained from the 3 land covers and the RMS of LAI time series. The mean time correlation is represented in black, with the dispersion in shaded grey area. The RMS is plotted in red. In addition, mean correlations for each 4 dominants PFTs in Europe are superimposed to the figure: DBF ($\circ$), ENF ($\square$), Crops (∇), Grass ($*$). The mean correlation decreases with smaller PFT percentage, and RMS increases. It implies that land cover differences have little to no impact on the OLS solution for the dominant PFTs, but that it has a big impact on the less dominant PFTs. Uncertainty in land cover impacts less the crops class than ENF compared to the mean.

As we chose a 3×3 pixels neighbourhood for the OLS, we tested the effect of the land cover differences on a 5×5 and 7×7 neighbourhood over the same 120 pixels in Europe. As shown in Fig. 6, enlarging the neighbourhood for OLS resolution lessened the impact of land cover uncertainty: the correlation decreases to 0.5 for very small PFT percentages. The effect of enlarging to 7×7 has no big impact compared to 5×5.

HESSD
8, 9113–9171, 2011

This could be caused by a higher variability of one PFT property, as suggested in the next paragraphs.

In addition to the land cover assumption, we assumed LAI for a PFT to be the same in the OLS neighbourhood, LAI_{PFT}. Some reasoning has been invoked previously to justify the assumption, but there is still variation because of the definition of PFTs itself: a PFT is a *class* of vegetation (Alton, 2011; Williams et al., 2009), and therefore could be different from one pixel to another. To check the realism of the hypothesis, we have analysed a set of LSA-SAF LAI images, one PFT at a time. For a given PFT, we consider for the analysis only the homogeneous pixels Hg, i.e. PFT covers more than 99 % of the surface. The LAI value for Hg is noted LAI_{Hg}. A sample *Ref* of this population is selected randomly to be reference values for LAI, LAI_{Ref}. The difference is computed between LAI_{Ref} and LAI_{Hg}, giving a probability density function (PDF) of the PFT LAI variability in function of the distance to the reference. As we study the implication of the OLS neighbourhood, we limit the analysis to a distance of 3 pixels from a reference, leaving three sizes denoted 3×3, 5×5 and 7×7. The PDFs are nearly symmetric and unimodal, very close to a gaussian (not shown). For further analysis, we therefore concentrate on the normalized standard deviation, as a proxy for the uncertainty.

For each PFT represented as Hg in Europe and Africa, the normalized standard deviation increases with the OLS neighbourhood size (Fig. 7). For Europe, the variability inside 3×3 neighbourhood range between 13 % and 19 %. Increasing the pixel number to 5×5 degrades the quality of the assumption for all PFTs. The variability increases gradually from 3×3 to 7×7 for C3 crops and Grasslands. For Africa, the uncertainty is much less than for Europe, ranging between 5 % and 9 % for all classes in the case of the 3×3 neighbourhood. In addition, enlarging the neighbourhood to 5×5 or 7×7 has no big impact for most PFTs in Africa, except for Grassland in Northern Africa. Variability could not be assessed for DBF over Africa, because no african ecosystem defined in ECOCLIMAP-I is homogeneous in that PFT.

HESSD
8, 9113–9171, 2011

For operational purpose, a robust estimate has to be delivered. We have concluded that using OLS method over a larger neighbourhood, i.e. more pixels, leads to a more robust estimate. However, we have shown that, at least for Europe, LAI variability of a given PFT increases with the size of the neighbourhood. Therefore, depending on the application to be made, a compromise has to made between accuracy and robustness. In applications involving spatial resolution equal to MSG/SEVIRI, the smallest size would obviously be preferred since it implies less uncertainty. However, it has been shown that the quality of the OLS algorithm is decreasing along with PFT occupation fraction, due to the land cover uncertainty. Therefore, a post-processing procedure has to be applied. Even if the contribution of small PFT percentages to the total surface fluxes are low, additional corrections are needed to have more reliable LAI time series. It is especially relevant for a proper in-situ validation, which is more meaningful if observations are compared to simulations at PFT level (Ghilain et al., 2011). To correct the estimates associated with small percentages, we have to implement a post-processing procedure using a reference estimate. That reference could be the LAI pixel value (option 1), or the LAI value corresponding to the closest pixel homogeneous for that PFT (option 2). Since african ecosystems are mostly mixed of PFTs, the first option is adopted for Africa. For Europe, clear homogeneous PFTs can be identified and isolated, and the second option is preferred. However, we should evaluate the implication of that latter option. In Fig. 8, the variability of LAI in function of the distance to the reference pixel is shown for each dominant PFT in Europe. A sliding average window of 5 distance units has been applied on the curve. As we could expect, the relative variability increases with the distance for every PFT, with the sharpest difference within the 5 first pixels. As well, the total increase is most important for grasslands (up to 55 % variability 30 pixels away) and crops (45 %), while it is less for forests (32 % and 37 %). The implication for the post-processing procedure is that the farther Hg used for correcting the OLS solution comes from, the more we introduce error, especially for crops and grasslands.

HESSD
8, 9113–9171, 2011

In regard to the estimation of the variability with the distance, we have represented in Fig. 9 the distribution of distance from each pixel to the closest Hg pixel for the same PFTs in Europe. For every PFT, the number of occurence decreases with the distance. The decrease is sharp for C3 crops, with more than 70 % of Hg no further than 6 pixels. For the other types, there are less Hg pixels and more localized by spots, and the decrease is quasi linear. In 90 % of the cases, Hg pixel is found at a distance of 16 pixels (Crops), 30 (ENF), 31 (G), and 33 (DBF). From Figs. 8 and 9, we conclude that the most uncertain correction in the post-processing will be for grasslands in Europe. In that specific case, correction must be done in another way, by applying the first option of postprocessing. As well, for PFTs which are not found as Hg in the neighbourhood, the first option is applied.

Based on the results we obtained in the present section, we choose the correction of LAI_{PFT} using LAI_{Hg} estimates (option 2) to be proportional to the PFT percentage α, obtained by linear regression of Fig. 5.

$$LAI_{PFT,PostP} = \alpha \cdot LAI_{PFT} + (1-\alpha) \cdot LAI_{Hg} \quad (17)$$

where α is the function

$$\alpha = \min(0.75 \cdot PFT_{\%} + 0.32, 1) \quad (18)$$

The final post-processing scheme proposed, P3, following P1 and P2, is summarized by a flowchart in Fig. 10. If the area to process is Europe, C3 crops, and forests (DBF and ENF) LAIs are corrected using option 2. For grassland, if the distance to Hg is higher than 10 pixels, the pixel LAI is used to correct (option 1). For other PFT classes, i.e. C4 crops, Irrigated crops and Swamp areas, correction follows option 1. For Africa, time series are less noisy, and no correction procedure is applied.

HESSD
8, 9113–9171, 2011

5 Comparison of ECOCLIMAP-I and processed LSA-SAF LAI: mean values, differences and uncertainties

5.1 Mean values and differences

The mean monthly LAI from ECOCLIMAP-I and LSA-SAF are compared by PFT (Fig. 11) in Europe for March to November 2007. Each monthly LAI is based on Hg pixels and six files per month are used to make the statistics. In addition to the mean monthly LAI, the LAI variability, spatial and temporal within a month for LSA-SAF, is estimated. From Fig. 11, it is shown that ECOCLIMAP-I LAI has a bias of about 1 m^2 m^{-2} compared to LSA-SAF LAI. That is especially visible for ENF during the summer months (∘) and crops for beginning of autumn (∘, ▽). This bias had also been reported in comparison with other products and in-situ data (Garrigues et al., 2008). A larger variability is found in LSA-SAF LAI for Swamp areas (Bogs), forests (DBF, ENF) and partly for grasslands (G). For crops, the variability is comparable.

Spatially, LSA-SAF LAI provides more variability compared to ECOCLIMAP-I, and especially for Africa. A probable explanation is that there are more defined ecosystems for Europe than for Africa, in the database. As an example, we compare the variability of PFTs issued from 3 different ECOCLIMAP-I classified ecosystems using LSA-SAF LAI and ECOCLIMAP-I LAI. The 3 homogeneous ecosystems are Tropical African grassland (ECOCLIMAP-I code: 88), Semi arid African grassland (89), and Nile Valley and desertic crops (105). Three LSA-SAF LAI images are selected for the comparison in 3 different months (15 April, 15 August and 15 December), and the LAI distribution is compared to the single value given by ECOCLIMAP-I monthly estimates (Fig. 12). Only the MSG pixels homogeneous in those PFTs have been used. For ecosystem 88, LAI given by ECOCLIMAP-I ranges between 2.0 and 3.0, while LSA-SAF LAI gives in one image a distribution ranging between 0 and 4. For the ecosystem 105, LSA-SAF LAI analysis shows a double peaked distribution, poorly represented by the LAI climatology of ECOCLIMAP-I. The difference is especially striking for April. ECOCLIMAP-I

HESSD
8, 9113–9171, 2011

gives a LAI of 0.5, while the peak reaches its maximum around 2.8. Those differences will inevitably impact on land surface model applications at MSG/SEVIRI scale.

Temporally, LSA-SAF LAI product allows a better representation of the inter-annual LAI evolution. As an example, we compare the LAI time series from ECOCLIMAP-I and LSA-SAF over a pixel in Western Africa corresponding to the ground measurement station Agoufou (15.29° N, 1.49° W) for 2007, 2008 and 2009. The variability is mostly driven by the occurence of rain during the wet season. In the comparison LSA-SAF LAI has been processed through the procedure described above, while ECOCLIMAP-I LAI has been rescaled to the range of LSA-SAF LAI, and linearly interpolated. In Fig. 13, we observe the time shifts in the wet season onset, as well as the differences in duration of that season and LAI peak. Differences up to 10 days in the shift are observed for the wet season onset (DoY 200–210). During the onset of the dry season (DoY 260–270), there is a large difference between ECOCLIMAP-I LAI and LSA-SAF LAI, with a sharp decrease of LSA-SAF LAI. Impact on the ET simulation with the land surface model is assessed in Sect. 6.

5.2 Uncertainties

While a thorough analysis of the uncertainty is out of the scope of the present paper, we compare rough estimates of LAI uncertainty for ECOCLIMAP-I, and LSA-SAF LAI, post-processed following our methodology, noted $\sigma_{\mathrm{LAI}_{\mathrm{ECO}}}$ and $\sigma_{\mathrm{LAI}_{\mathrm{SAF}}}$ respectively.

$\sigma_{\mathrm{LAI}_{\mathrm{SAF}}}$ is the combination (Eq. 19) of the error on OLS, σ_{OLS}, and the error on assumptions (equal LAI for a PFT in OLS neighbourhood), σ_{dist} (Fig. 7).

$$\sigma_{\mathrm{LAI}_{\mathrm{SAF}}} = \sqrt{\sigma_{\mathrm{dist}}^2 + \sigma_{\mathrm{OLS}}^2} \tag{19}$$

$\sigma_{\mathrm{LAI}_{\mathrm{ECO}}}$ can be evaluated through the analysis of the spatial and temporal variability of LSA-SAF LAI for a given PFT and a given month for each ECOCLIMAP-I ecosystem.

For Europe, we have shown in Sect. 4.3 that LAI variability for a given PFT increases with the distance from a reference pixel. But, while for forests the variability remains

HESSD
8, 9113–9171, 2011

almost steady with the distance, crops and grasslands are the most affected PFTs, giving a clear methodological advantage in using LSA-SAF LAI and an expected lower uncertainty. However, since ECOCLIMAP-I proposes a very fine classification into 92 ecosystems, e.g. 27 different types of crops and 21 types of grasslands, the difference between $\sigma_{\mathrm{LAI}_{\mathrm{SAF}}}$ and $\sigma_{\mathrm{LAI}_{\mathrm{ECO}}}$ is not expected to be large.

For Africa, Fig. 12 shows examples representative of wide areas in NAfr region for a given year (2007). Consequently, the deduced $\sigma_{\mathrm{LAI}_{\mathrm{ECO}}}$ can be very large. Contrarily, $\sigma_{\mathrm{LAI}_{\mathrm{SAF}}}$ is expected to be much less, because σ_{dist} is less than 10 %, and σ_{OLS} is very small due to the relative homogeneity of the landscape over the OLS neighbourhood. Especially, $\sigma_{\mathrm{LAI}_{\mathrm{SAF}}}$ is expected to be much smaller than $\sigma_{\mathrm{LAI}_{\mathrm{ECO}}}$ in semi-arid to arid environments in Africa, giving a more reliable LAI estimate for Sahel. That difference should obviously be exacerbated if we take into account the inter-annual variability not represented in ECOCLIMAP-I, as in Fig. 13.

6 Impact on the half-hourly latent heat flux and the daily evapotranspiration rate

The impact of using LSA-SAF LAI instead of ECOCLIMAP-I database in the land surface model is evaluated at different observation sites, equipped with eddy covariance devices. Results of point scale simulations are compared to in-situ observations of latent heat flux, LE (list of stations in Table 3). Four sites are situated in Africa and five in Europe, with a good sample of different climates. The four sites in Africa are installed in a savannah landscape, but with different precipitation regimes, ranging from mostly dry (Agoufou) to mostly wet (Tchizalamou). The European sites are situated in mediterranean (Puéchabon and Tojal), temperate (Vielsalm and Wetzstein) and boreal (Sodankylä) regions. Four European stations monitor the exchanges between a forest stand and the atmosphere: coniferous forest (Wetzstein and Sodankylä), evergreen forest (Puéchabon) and mixed forest (Vielsalm). The station of Tojal monitors exchanges over a C3/C4 grassland site. Most of the sites selected have a large homogeneous fetch, that allows a good representativity of the measurements.

HESSD
8, 9113–9171, 2011

The model is forced by meteorological variables from ERA-Interim (Simmons et al., 2006), interpolated in time (30 min). In order to better assess the impact of LAI on the simulations, radiation forcing are the in-situ measurements, and observed precipitation, if available. If not available, radiation forcing are the LSA-SAF estimates (DSSF and DSLF), and precipitation rates are ERA-Interim re-analyses. Precipitation is especially important in semi-arid environment (Merbold et al., 2009), and the more accurate the input is the better is the model output. Soil moisture and soil temperature for the four soil layers are initialized with ERA-Interim analysis, and the model is run over one year before the analyzed run. Model parameters are not tuned for the selected sites, and the general parameterization for a global simulation is set.

Statistical results for the 30 min LE are presented in Table 4. Statistical scores show an improvement in the modeling of the surface latent heat flux, especially for semi-arid regions where the signal shows an interannual variability in amplitude and phase. The largest improvements are observed for Skukuza and Agoufou sites, with a significant decrease of the global bias compared to data (-37 to $-6\,W\,m^{-2}$ for Skukuza, and -32 to $-18\,W\,m^{-2}$ for Agoufou), as well as an improved Nash-Sutcliffe (NS) index (0.46 to 0.60, and 0.26 to 0.45, respectively) (Nash and Suttcliffe, 1970). Even if the scores are largely improved in the Agoufou comparison, most of the remaining bias is due to non ideal precipitation forcing, i.e. ERA-Interim in that simulations. The other simulations over african sites, i.e. Demokeya and Tchizalamou, also show an improvement of the statistical scores when compared to data (NS: 0.53 to 0.62, and 0.51 to 0.53, respectively). Those results confirm the findings of Kahan et al. (2006), over the Sahel region in Western Africa.

As an example, we present in Fig. 14 the time series of the simulated and observed LE in Demokeya for the year 2007 to 2009. The simulation is clearly improved with the use of LSA-SAF LAI, with a better match during the wet season. Also the simulations of LE during the dry season is closer to the observations.

Results over Europe show an improvement for 3 sites over the 5. In Puéchabon, the scores are well improved, with a global bias reduction, from -9 to $3\,W\,m^{-2}$, and a better

HESSD
8, 9113–9171, 2011

NS, from 0.61 to 0.67. As well, the results are improved for 2 forested sites in different climates, i.e. Wetzstein and Sodankylä. For Tojal and Vielsalm, the model perform well with ECOCLIMAP-I and the statistics are either slightly degraded or equal.

Based on the comparison of LAI from the two sources, the greatest impact is expected in Africa. There is a growing interest in the land surface monitoring in Western Africa, where quantitative remote sensing is expected to play an important role. Especially, surface heat fluxes, evapotranspiration and carbon fluxes are now under focus in different projects (Stisen et al., 2008; Boone et al., 2009). In that perspective, and for a better evaluatation of the spatial impact of using ECOCLIMAP-I or LSA-SAF LAI, we compare the simulations along a North-South transect in West Africa, 15° N to 6° N, 0° E, for the year 2007. The evolution of the LAI on the latitude gradient is shown in Fig. 15 for monthly ECOCLIMAP-I and daily LSA-SAF. The northern bound of the transect is completely arid with no vegetation. Southwards, vegetation is seasonal, with longer periods of vegetation cover, and higher amplitudes. The global pattern for ECOCLIMAP-I and LSA-SAF is similar, however, the most striking difference is seen on the length of the vegetation period, that is noticeably shorter for LSA-SAF at highest latitudes. Between 6° N and 8° N, the transect meets lakes, resulting in zero LAI as observed from the dark blue stripes in the figures.

The land surface model is forced by ERA-Interim re-analysis meteorological surface fields, i.e. air temperature, air humidity, wind speed, precipitation, interpolated in time (30 min). Radiation forcing, i.e. short and long wave downward radiation at the surface, as well as the surface albedo, is given by LSA-SAF, respectively half-hourly DSSF and DSLF, and daily ALBEDO products. Half-hourly simulated LE are converted to evapotranspiration rates and daily cumulated. The evolution for 2007 along the transect is shown in Fig. 16, when using ECOCLIMAP-I and LSA-SAF LAI respectively. The global pattern is mostly the same, as ET is driven by precipitation. However, large differences are found between October and December, with higher ET produced using ECOCLIMAP-I database.

HESSD
8, 9113–9171, 2011

Beside a direct comparison of ET, we can assess the impact of using LSA-SAF LAI in the land surface model by comparing to complementary remote sensing derived data. The land surface temperature derived from satellites is said to be related to the soil water content, and could therefore be suitable to compare with the *skin* temperature used in land surface models. Even if the model *skin* temperature has not the exact same physical meaning as the radiative land surface temperature measured by the satellite, it is often considered to be comparable (e.g. Ghent et al., 2011). LSA-SAF provides land surface temperature images, LSA-SAF LST, every 15 min, based on MSG/SEVIRI, at the sensor resolution (Trigo et al., 2008). Daily surface heating rates, expressed in $K\,h^{-1}$, are calculated from LSA-SAF 15 min LST data, and from the simulated 30 min skin temperature separately. The heating rates are the slope of the linear fit through the land surface temperature data between sunrise and local noon. The resulting heating rates are shown in Fig. 17. Vegetated areas are characterized by lower mean surface heating rates than bare soil. As well, surface heating rates are said to be increased with decreasing soil moisture (Stisen et al., 2008). The global pattern with the contrast low/high heating rate is seen in the 3 images. Good correspondance is found in the patterns of both simulations. That is probably due to the same precipitation forcing for the model. The absolute differences between simulated heating rates and those derived from LSA-SAF LST are represented in Fig. 18. A closer agreement with a lower bias is found with the skin temperature simulated using LSA-SAF LAI than with ECOCLIMAP-I when compared to LSA-SAF derived heating rates, suggesting than simulation is improved using LSA-SAF LAI.

7 Discussion: land covers and applicability to evapotranspiration monitoring in near-real time

The scheme presented here has been developed to comply with requirements for near-real time applications, and allows the use LSA-SAF LAI and FVC from 2007 onwards for ET monitoring at spatial scales equal or coarser than MSG/SEVIRI using a land

HESSD
8, 9113–9171, 2011

surface model. However, critical points dealing with needed auxiliary information on land cover have been rised in Sect. 4.3. Particularly, for a correct evaluation of LAI at PFT level, it is expected to use a land cover, that proposes a sufficient accuracy in locating, classifying and decomposing into PFTs accepted by the land surface models. The gain in spatial resolution (ECOCLIMAP-I: 1 km; GlobCover: 300 m) and passage frequency of the satellites over the same location are clear advantages to obtain more accurate LAI at PFT level, and therefore an optimal input for land surface models.

For near-real time ET monitoring using land surface models, we have shown that using daily remote sensing derived LAI is useful. As well, in line with the monitoring concept, it would be necessary to have a clear assessment of the land cover changes, as it can affect our scheme. Regular updates of land cover would therefore be appreciated, to address land conversion issues like deforestation or fires. Two land covers used in our study, GlobCover and MCD12Q1, propose updates, even if classification updates in heteorogeneous landscapes using available methodologies still remain uncertain (Bontemps et al., 2011).

For continuous monitoring using MSG satellites that are expected to last at least until the launch of MTG satellites foreseen in 2017, the use of successive satellites for global vegetation monitoring are of high interest, since new land cover maps could be produced and possibly cross-checked. GlobCover maps have been produced from MERIS data, MCD12Q1 yearly maps are derived from MODIS/Aqua and Terra spectral data, and ECOCLIMAP-II, the upcoming update of ECOCLIMAP-I, is based on SPOT-VEGETATION data. However, those sensors have past their planned life time, or will do soon, and new data are expected to create a consistent and updated suite of land covers. While Sentinel-3 suite of satellites is highly expected for global land surface monitoring, the mission has a probable launch in 2013. Within the GMES initiative, PROBA-V (Mellab, 2009) has been conceived as a *gap filling mission* between the VEGETATION and the Sentinel-3 programs, to avoid any gap in the global remote sensing monitoring of the vegetation. Besides its role of continuation mission from VEGETATION (resolution of approximately 1 km), PROBA-V, with an expected nominal

HESSD
8, 9113–9171, 2011

life time of minimum 2.5 to 5 yr, will monitor the land surface with an enhanced spatial resolution to 330 m and a global coverage every day for latitudes beyond 35° and 90 % coverage for equatorial regions, giving a chance to derive a land cover accurate enough for ET monitoring at MSG spatial resolution for the gap period.

8 Conclusions

We propose a practical methodology to use the biophysical products LSA-SAF LAI and FVC issued from the geostationary meteorological satellite MSG/SEVIRI, in land surface models, and explore its utility for the monitoring of surface turbulent fluxes compared to the use of a semi-static vegetation database, e.g. ECOCLIMAP-I. After an optimal interpolation of LAI with a climatology at pixel level, a simple OLS method using a land cover helps in downscaling LSA-SAF LAI to the PFT level. Effects of spatial scale and land cover differences have been investigated, and results show that land cover uncertainty has an increasing impact on the less represented PFTs in a pixel using a group on 3×3 pixels. The impact lowers when enlarging to 5×5 or 7×7 pixels. Those results imply that the simple method is more robust as the spatial scale considered is coarser. However, we propose a scheme to correct the errors due to land cover uncertainty for monitoring at the finest scale possible, taking into account the uncertainty assumptions.

LAI maps from LSA-SAF and ECOCLIMAP-I are compared at different time and spatial scales. We have shown that ECOCLIMAP-I LAI presents less variability than LSA-SAF LAI, with respect to spatial coverage and temporal frequency. In addition, there is a bias of nearly $1\,m^2\,m^{-2}$ between both sources. A rough analysis of the uncertainty on ECOCLIMAP-I LAI and LSA-SAF LAI over Africa gives a hint that LSA-SAF LAI is more suited for land surface models intended for daily time scales at MSG/SEVIRI resolution.

We have assessed the impact of using LSA-SAF LAI instead of ECOCLIMAP-I in a land surface model run at MSG/SEVIRI resolution. Statistical scores of the comparison

HESSD
8, 9113–9171, 2011

between the simulations and latent heat flux observations from ground measurement sites over Europe and Africa are improved in most cases, and especially in semi-arid climates. Amplitudes of anual cycles, as well as phase shifts are more correctly taken into account in the model compared to the use of the database.

A simulation over a North-South transect in Western Africa using LSA-SAF radiation products and ERA-Interim meteorological variables, illustrates the impact of using LSA-SAF vegetation parameters compared to ECOCLIMAP-I database. The result is assessed through a comparison of the simulated skin temperature daily heating rates with observed land surface temperature heating rates from MSG/SEVIRI, and we have observed a better global agreement by using LSA-SAF vegetation parameters for the land surface model simulation.

Use of LSA-SAF LAI and FVC is therefore recommended for near-real time applications of land surface models working at the MSG/SEVIRI scale and intending at monitoring daily evapotranspiration. Especially, it will improve the land surface model applications over Africa.

Acknowledgements. The authors thank F. J. Garcia-Haro, F. Camacho de Coca and the LSA-SAF operating team to provide the LSA-SAF LAI and FVC images in near-real time, as well as DSSF, DSLF and ALBEDO. We also thank G. Balsamo for providing the H-TESSEL code, the in-situ data providers who could provide us with the necessary material for benchmarking, and ESA Globcover Project led by MEDIAS France for providing the Globcover land cover. The MODIS MCD12Q1 data were obtained through the online Data Pool at the NASA Land Processes Distributed Active Archive Center (LP DAAC), USGS/Earth Resources Observation and Science (EROS) Center, Sioux Falls, South Dakota (http://lpdaac.usgs.gov/get_data). This study has been done in the framework of the LSA-SAF project, funded at RMI by EUMETSAT and by ESA (contract e15066) under the PRODEX-9 programme supported by the Belgian Sciences Policy, and in the framework of PROBA-VET project, supported by the Belgian Science Policy through the PROBA-V preparatory programme (contract CB/34/18).

HESSD
8, 9113–9171, 2011

References

ALADIN International Team, The ALADIN project: Mesoscale modelling seen as a basic tool for weather forecasting and atmospheric research, WMO Bull., 46, 317–324, 1997. 9117

Albergel, C., Calvet, J.-C., Mahfouf, J.-F., Rüdiger, C., Barbu, A. L., Lafont, S., Rouhean, J.-L., Walker, J. P., Crapeau, M., and Wigneron, J.-P.: Monitoring of water and carbon fluxes using a land data assimilation system: a case study for southwestern France, Hydrol. Earth Syst. Sci., 14, 1109–1124, doi:10.5194/hess-14-1109-2010, 2010. 9115, 9116

Alton, P. B.: How useful are plant functional types in global simulations of the carbon, water, and energy cycles?, J. Geophys. Res., 116, G01030, doi:10.1029/2010JG001430, 2011. 9130

Anderson, M. C., Norman, J. M., Mecikalski, J. R., Otkin, J. A., and Kustas, W. P.: A climatological study of evapotranspiration and moisture stress across the continental United States based on thermal remote sensing: 1. Model formulation, J. Geophys. Res., 112, D10117, doi:10.1029/2006JD007506, 2007.

Aubinet, M., Chermanne, B., Vandenhaute, M., Longdoz, B., Yernaux, M., and Leitat, E.: Long term carbon dioxide exchange above a mixed forest in the Belgian Ardennes, Agr. Forest Meteorol., 108, 293–315, 2001. 9152

Balsamo, G., Viterbo, P., Beijaars, A., van den Hurk, B., Hirschi, M., Betts, A. K., and Scipal, K.: A revised hydrology for the ECMWF model: Verification from field site to terrestrial water storage and impact in the integrated forecast system, J. Hydrometeorol., 10, 623–643, 2009. 9115, 9120, 9121

Baret, F., Hagolle, O., Geiger, B., Bicheron, P., Miras, B.,Huc, M., Berthelot, B., Nino, F.,Weiss, M., Samain, O., Roujean, J. L., and Leroy, M.: LAI, FAPAR, and FCover CYCLOPES global products derived from Vegetation. Part 1: principles of the algorithm, Remote Sens. Environ., 110, 305–316, 2007. 9117

Bartholomé, E. and Belward, A. S.: GLC2000: a new approach to global land cover mapping from Earth observation data, Int. J. Remote Sens., 26, 9, 1959–1977, doi:10.1080/01431160412331291297, 2005. 9118

Beljaars, A. C. M. and Viterbo, P.: The sensitivity of winter evaporation to the formulation of aerodynamic resistance in the ECMWF model, Bound.-Lay. Meteorol., 71, 135–149, 1994. 9120

Bicheron, P., Leroy, M., Brockmann, C., Krämer, U., Miras, B., Huc, M., Nino, F., Defourny, P., Vancutsem, C., Arino, O., Ranéra, F., Petit, D., Amberg, V., Berthelot, B., and Gross,

HESSD
8, 9113–9171, 2011

D.: GLOBCOVER : a 300m global land cover product for 2005 using ENVISAT/MERIS time series, Proceedings of the Recent Advances in Quantitative Remote Sensing Symposium, Valencia, September 2006. 9118

Bicheron, P., Huc, M., Henry C., Bontemps, S., and GLOBCOVER partners: GLOBCOVER: Products Description Manual, GLOBCOVER-PDM-I2.2, 2008. 9118

Blyth, E., Best, M., Cox, P., Essery, R., Boucher, O., Harding, R., Prentice, C., Vidale, P. L., and Woodward, I.: JULES: a new community land surface model, Global Change NewsLetter, 66, 9–11, 2006. 9115

Bonan, G. B., Levis, S., Kergoat, L., and Oleson, K. W.: Landscapes as patches of plant functional types: An integrated concept for climate and ecosystem models, Global Biogeochem. Cy., 16, 1021, doi:10.1029/2000GB001360, 2002. 9121

Bontemps, S., Herold, M., Kooistra, L., van Groenestijn, A., Hartley, A., Arino, O., Moreau, I., and Defourny, P.: Revisiting land cover observations to address the needs of the climate modelling community, Biogeosciences Discuss., 8, 7713–7740, doi:10.5194/bgd-8-7713-2011, 2011. 9139

Boone, A., de Rosnay, P., Balsamo, G., Beljaars, A., Chopin, F., Decharme, B., Delire, C., Ducharme, A., Gascoin, S., Grippa, M., Guichard, F., Gusev, Y., Harris, P., Jarlan, L., Kergoat, L., Mougin, E., Nasonova, O., Norgaard, A., Orgeval, T., Ottle, C., Poccard-Leclercq, I., Polcher, J., Sandholt, I., Saux-Picart, S., Taylor, C. and Xue, Y.: The AMMA Land Surface Model Intercomparison Project (ALMIP), B. Am. Meteorol. Soc., 90, 1865–1880, 2009. 9119, 9137

Brut, A., Rüdiger, C., Lafont, S., Roujean, J.-L., Calvet, J.-C., Jarlan, L., Gibelin, A.-L., Albergel, C., Le Moigne, P., Soussana, J.-F., Klumpp, K., Guyon, D., Wigneron, J.-P., and Ceschia, E.: Modelling LAI at a regional scale with ISBA-A-gs: comparison with satellite-derived LAI over southwestern France, Biogeosciences, 6, 1389–1404, doi:10.5194/bg-6-1389-2009, 2009. 9115

Brutsaert, W. H.: Evaporation in the Atmosphere – Theory, History, and Applications. Kluwer Academic, D. Reidel publishers, Dordrecht, The Netherlands, 299 pp., 1982. 9118

Carrer, D., Roujean, J.-L., and Meurey, C.: Comparing Operational MSG/SEVIRI Land Surface Albedo Products From Land SAF With Ground Measurements and MODIS, IEEE T. Geosci. Remote, 48, 1714–1728, doi:10.1109/TGRS.2009.2034530, 2010. 9122

Champeaux, J. L., Masson, V., and Chauvin, F.: ECOCLIMAP: a global database of land surface parameters at 1 km resolution, Meteorol. Appl., 12, 29–32,

HESSD

8, 9113–9171, 2011

doi:10.1017/S1350482705001519, 2005. 9117
Chen, J. M., Menges, C. H., and Leblanc, S.: Global derivation of the vegetation clumping index from multi-angular satellite data, Remote Sens. Environ., 97, 447–457, 2005. 9118
Cooley, H. S., Riley, W. J., Torn, M. S., and He, Y.: Impact of agricultural practice on regional climate in a coupled land surface mesoscale model, J. Geophys. Res., 110, D03113, doi:10.1029/2004JD005160, 2005. 9120
Courault, D., Seguin, B., and Olioso, A.: Review on estimation of evapotranspiration from remote sensing data: from empirical to numerical modelling approaches, Irrig. Drain., 19, 223–249, 2005. 9114
Dorigo, W. A., Zurita-Milla, R., De Wit, A. J. W., Brazile, J., Singh, R., and Schaepman, M.E.: A review on reflective remote sensing and data assimilation techniques for enhanced agroecosystem modeling, Int. J. Appl. Earth Obs., 9, 165–193, 2006. 9115
ECOCLIMAP-I database: http://www.cnrm.meteo.fr/gmme/PROJETS/ECOCLIMAP/page_ecoclimap.htm, last access: 8 September 2011, 2006. 9151
Faroux, S., Masson, V., and Roujean, J.-L.: ECOCLIMAP-II: a climatologic global data base of ecosystems and land surface parameters at 1 km based on the analysis of time series of VEGETATION data, Geosci. Remote. Sens. Symp, IGARSS2007, IEEE International, 23–28 July 2007, Barcelona, 1008–1011, 2007. 9117
García-Haro, F. J., Camacho-de Coca, F., Meliá, J., and Martínez, B.: Operational derivation of vegetation products in the framework of the LSA SAF project, Proceedings of the EUMETSAT Meteorological Satellite Conference, Dubrovnik (Croatia), 19–23 September, 2005a. 9119
García-Haro, F. J., Sommer, S., and Kemper, T.: Variable multiple endmember spectral mixture analysis (VMESMA), Int. J. Remote Sens., 26, 2135–2162, 2005b. 9119
Garrigues, S., Lacaze, R., Baret, F., Morisette, J. T., Weiss, M., Nickeson, J. E., Fernandes, R., Plummer, S., Shabanov, N. V., Myneni, R. B., Knyazikhin, Y., and Yang, W.: Validation and intercomparison of global Leaf Area Index products derived from remote sensing data, J. Geophys. Res., 113, G02028, doi:10.1029/2007JG000635, 2008. 9133
Ge, J.: On the proper use of satellite-derived leaf area index in climate modeling, J. Climate, 22, 4427–4433, doi:10.1175/2009JCLI2868.1, 2009. 9128
Geiger, B., Carrer, D., Franchistéguy, L., Roujean, J.-L., and Meurey, C.: Land Surface Albedo derived on a daily basis from Meteosat Second Generation Observations, IEEE T. Geosci. Remote, 46, 3841–3856, 2008a. 9122
Geiger, B., Meurey, C., Lajas, D., Franchistéguy, L., Carrer, D., and Roujean, J.-L.: Near real

HESSD
8, 9113–9171, 2011

time provision of downwelling shortwave radiation estimates derived from satellite observations, Meteorol. Appl., 15, 411–420, 2008b. 9122
Ghent, D., Kaduk, J., Remedois, J., and Balzter, H.: Data assimilation into land surface models: the implications for climate feedbacks, Int. J. Remote Sens., 32, 617–632, doi:10.1080/01431161.2010.517794, 2011. 9138
Grippa, M., Kergoat, L., Frappart, F., Araud, Q., Boone, A., de Rosnay, P., Lemoine, J.-M., Gascoin, S., Balsamo, G., Ottle, C., Decharme, B., Saux-Picart, S., and Ramillien, G.: Land water storage variability over West Africa estimated by Gravity Recovery and Climate Experiment (GRACE) and land surface models, Water Resour. Res., 47, W05549, doi:10.1029/2009WR008856, 2011. 9119
Gibelin, A.-L., Calvet, J.-C. Roujean, J.-L., Jarlan, L., and Los, S. O.: Ability of the land surface model ISBA-A-gs to simulate leaf area index at the global scale: Comparison with satellites products, J. Geophys. Res., 111, D18102, doi:10.1029/2005JD006691, 2006. 9115
Ghilain, N., Arboleda, A., and Gellens-Meulenberghs, F.: Evapotranspiration modelling at large scale using near-real time MSG SEVIRI derived data, Hydrol. Earth Syst. Sci., 15, 771–786, doi:10.5194/hess-15-771-2011, 2011. 9121, 9122, 9129, 9131
Gobron, N., Pinty, B., Aussedat, O., Chen, J.M., Cohen, W.B., Fensholt, R., Gond, V., Huemmrich, K.F., Lavergne, T., Malin, F., Privette, J.L., Sandholt, I., Taberner, M., Turner, D.P., Verstraete, M.M., and Widlowski, J.-L.: Evaluation of fraction of absorbed photosynthetically active radiation products for different canopy radiation transfer regimes: Methodology and results using Joint Research Center products derived from Sea- WiFS against ground-based estimations, J. Geophys. Res., 111, D13110, doi:10.1029/2005JD006511, 2006. 9117
Granier, A., Biron, P., and Lemoine, D.: Water balance, transpiration and canopy conductance in two beech stands, Agr. Forest Meteorol., 100, 291–308, 2000. 9129
Gu, Y., Bélair, S., Mahfouf, J.-F., and Deblonde, G.: Optimal interpolation analysis of leaf area index using MODIS data, Remote Sens. Environ., 104, 283–296, doi:10.1016/j.rse.2006.04.021, 2006. 9123, 9124, 9125
Ineichen, P., Barroso, C. S., Geiger, B., Hollmann, R., Marsouin, A., and Mueller, R.: Satellite Application Facilities irradiance products: hourly time step comparison and validation over Europe, Int. J. Remote Sens., 30, 5549–5571, doi:10.1080/01431160802680560, 2009. 9122
Jarlan, L., Balsamo, G., Lafont, S., Beljaars, A., Calvet, J.-C., and Mougin, E.: Analysis of leaf area index in the ECMWF land surface model and impact on latent heat and carbon fluxes:

HESSD
8, 9113–9171, 2011

Application to West Africa, J. Geophys. Res. D, 113, D24117, doi:10.1029/2007JD009370, 2008. 9115
Jarvis, P. G.: The interpretation of the variations in leaf water potential and stomatal conductance found in canopies in the field, Phil. Trans. Roy. Soc. London, B273, 593–610, 1976.
Jiang, L., Kogan, F. N., Guo, W., Tarpley, J. D., Mitchell, K. E., Ek, M. B., Tian, Y., Zheng, W., Zou, C.-Z., and Ramsay, B. H.: Real-time weekly global green vegetation fraction derived from advanced very high resolution radiometer-based NOAA operational global vegetation index (GVI) system, J. Geophys. Res., 115, D11114, doi:10.1029/2009JD013204, 2010. 9124, 9127
Joffre, R., Rambal, S., and Romane, F.: Local variations of ecosystem functions in a Mediterranean evergreen oak woodland, Ann. For. Sci., 53, 561–570, 1996. 9152
Jung, M., Henkel, K., Herold, M., and Churkina, G.: Exploiting synergies of global land cover products for carbon cycle modeling, Remote Sens. Environ., 101, 534–553, doi:10.1016/j.rse.2006.01.020, 2006. 9129
Kahan, D. S., Xue, Y., and Allen, S. J.: The impact of vegetation and soil parameters in simulations of surface energy and water balance in the semi-arid sahel: A case study using SEBEX and HAPEX-Sahel data, J. Hydrol., 320, 238–259, doi:10.1016/j.jhydrol.2005.07.011, 2006. 9136
Kalma, J. D., McVicar, T. R., and McCabe, M. F.: Estimating Land Surface Evapotranspiration: A Review of Methods Using Remotely Sensed Surface Temperature Data, Surveys in Geophysics, 29, 421–469, doi:10.1007/s10712-008-9037-z, 2008. 9114
Kaptué Tchuente, A. T., Roujean, J.-L., and Faroux, S.: ECOCLIMAP-II: an ecosystem classification and land surface parameter database of Western Africa at 1 km resolution for the African Monsoon Multidisciplinary Analysis (AMMA) project, Remote Sens. Environ., 114, 961–976, 2010. 9118
Kaptué Tchuente, A. T., De Jong, S. M., Roujean, J.-L., Favier, C., and Mering, C.: Ecosystem mapping at the African continent scale using a hybrid clustering approach based on 1-km resolution multi-annual data from SPOT/VEGETATION, Remote Sens. Eviron., 115, 452–464, doi:10.1016/j.rse.2010.09.015, 2011.
Kato, H., Rodell, M., Beyrich, F., Cleugh, H., van Gorsel, E., Liu, H., and Meyers, T. P.: Sensitivity of Land Surface Simulations to Model Physics, Parameters, and Forcings, at Four CEOP Sites, J. Meteorol. Soc. Japan, 85A, 187–204, 2007.
Kutsch, W. L., Hanan, N., Scholes, B., McHugh, I., Kubheka, W., Eckhardt, H., and Williams,

HESSD
8, 9113–9171, 2011

C.: Response of carbon fluxes to water relations in a savanna ecosystem in South Africa, Biogeosciences, 5, 1797–1808, doi:10.5194/bg-5-1797-2008, 2008. 9152
LSA-SAF ET Team (Arboleda, A., Ghilain, N., and Gellens-Meulenberghs, F.): LSA-SAF Product User Manual Evapotranspiration (ET), PUM METv2.2, 33 pp, 2010.
Lawrence, P. J. and Chase, T. N.: Representing a new MODIS consistent land surface in the Community Land Model (CLM 3.0), J. Geophys. Res., 112, G01023, doi:10.1029/2006JG000168, 2007. 9119
LSA-SAF VEGA Team (Camacho-de-Coca, F., Garcia-Haro, F. J., Verger, A., and Melia, J.): LSA-SAF Product User Manual: Vegetation parameters (FVC, LAI, FAPAR), PUM-VEGAv2.1, 2008. 9116, 9120, 9124
Li, Z.-L., Tang, R., Wan, Z., Bi, Y., Zhou, C., Tang, B., Yan, G., and Zhang, X.: A review of current methodologies for regional evapotranspiration estimation from remotely sensed data, Sensors, 9, 3801–3853, doi:10.3390/s90503801, 2009. 9115
Loveland, T. R., Reed, B. C., Brown, J. F., Ohlen, D. O., Zhu, Z., and Yang, L.: Development of a global land cover characteristics database and IGBP DISCover from 1 km AVHRR data, Int. J. Remote Sens., 21, 1303–1330, 2000. 9118
Masson, V., Champeaux, J. L., Chauvin, F., Meriguet, Ch., and Lacaze, R. A.: Global database of land surface parameters at 1-km resolution in meteorological and climate models. J. Climate, 16, 1261–1282, 2003. 9117, 9119
Mellab, K.: PROBA-V Spacecraft and Vegetation Instrument Presentation, PROBA-V International Users Committee, Brussels, 14 December 2009, http://probav-iuc.org/assets/ProbaV-ESA_Presentation.pdf, 2009. 9139
Merbold, L., Ardö, J., Arneth, A., Scholes, R. J., Nouvellon, Y., de Grandcourt, A., Archibald, S., Bonnefond, J. M., Boulain, N., Brueggemann, N., Bruemmer, C., Cappelaere, B., Ceschia, E., El-Khidir, H. A. M., El-Tahir, B. A., Falk, U., Lloyd, J., Kergoat, L., Le Dantec, V., Mougin, E., Muchinda, M., Mukelabai, M. M., Ramier, D., Roupsard, O., Timouk, F., Veenendaal, E. M., and Kutsch, W. L.: Precipitation as driver of carbon fluxes in 11 African ecosystems, Biogeosciences, 6, 1027–1041, doi:10.5194/bg-6-1027-2009, 2009. 9136, 9152
Miller J., Barlage, M., Zeng, X., Wei, H., Mitchell, K., and Tarpley, D.: Sensitivity of the NCEP/Noah land surface model to the MODIS green vegetation fraction data set, Geophys. Res. Lett., 33, L13404, doi:10.1029/2006GL026636, 2006. 9128
Nash, J. E. and Suttcliffe, J. V.: River Flow Forecasting through Conceptual Models, Part I-A Discussion of Principles, J. Hydrol., 10, 282–290, 1970. 9136, 9153

HESSD
8, 9113–9171, 2011

Baret, F., O. Hagolle, B. Geiger, P. Bicheron, B. Miras, M.Huc, B. Berthelot, f. Nino, M.Weiss, O. Samain, J.L. Roujean, and M.Leroy, 2007: LAI, FAPAR, and FCover CYCLOPES global products derived from Vegetation. Part 1: principles of the algorithm, Rem. Sens. Environ., 110:305-316. 9115

Oleson, K. and Bonan, G.: The effects of remotely sensed plant functional type and leaf area index on simulations of boreal forest surface fluxes by the NCAR land surface model, J. Hydrometerol., 1, 431–446, 2000. 9127

Pereira, J. S., Mateus, J. A., Aires, L. M., Pita, G., Pio, C., David, J. S., Andrade, V., Banza, J., David, T. S., Paço, T. A., and Rodrigues, A.: Net ecosystem carbon exchange in three contrasting Mediterranean ecosystems the effect of drought, Biogeosciences, 4, 791–802, doi:10.5194/bg-4-791-2007, 2007. 9129, 9152

Rebmann, C., Zeri, M., Lasslop, G., Mund, M., Kolle, O., Schulze, E.-D., and Feigenwinter, C.: Treatment and assessment of the CO_2-exchange at a complex forest site in Thuringia, Germany, Agr. Forest Meteorol., 150, 684–691, 2010. 9152

Rodell, M., Houser, P. R., Jambor, U., Gottschalck, J., Mitchell, K., Meng, C.-J., Arsenault, K., Cosgrove, B., Radakovich, J., Bosilovich, M., Entin, J. K., Walker, J. P., Lohmann, D. and Toll, D.: The Global Land Data Assimilation System, B. Am. Meteorol. Soc., 85, 381–394, 2004. 9116

Sepulcre-Cantó, G., Gellens-Meulenberghs, F., Arboleda, A., Duveiller, G., De Wit, A., Eerens, H., Djaby, B., and Defourny, P.: Estimating crop specific evapotranspiration using remote sensing imagery at various spatial resolutions for improving crop growth modeling, Int. J. Remote Sens., accepted, 2011. 9120

Simmons, A., Uppala, S., Dee, D., and Kobayashi, S.: ERA-Interim: New ECMWF reanalysis products from 1989 onwards, ECMWF Newsletter, 10, 26–35, 2006. 9122, 9136

Sjöström, M., Ardö, J., Eklundh, L., El-Tahir, B. A., El-Khidir, H. A. M., Hellström, M., Pilesjö, P., and Seaquist, J.: Evaluation of satellite based indices for gross primary production estimates in a sparse savanna in the Sudan, Biogeosciences, 6, 129–138, doi:10.5194/bg-6-129-2009, 2009. 9152

Stisen, S, Sandholt, I., Noergaard, A., Fensholt, R. and Jensen, K.H.: Combining the triangle method with thermal inertia to estimate regional evapotranspiration – Applied to MSG-SEVIRI data in the Senegal River basin, Remote Sens. Environ., 110, 1242–1255, doi:10.1016/j.rse.2007.08.013, 2008. 9137, 9138

Suni, T., Berninger, F., Vesala, T., Markkanen, T., Pertti, H., Makela, A., Ilvesniemi, H., Hanni-

HESSD
8, 9113–9171, 2011

nen, H., Nikinmaa, E., Huttula, T., Laurila, T., Aurela, M., Grelle, A., Lindroth, A., Arneth, A., Shibistova, O., and Lloyd, J.: Air temperature triggers the recovery of evergreen boreal forest photosynthesis in spring, Global Change Biology, 9, 10, 1410–1426, doi:10.1046/j.1365-2486.2003.00597.x, 2003. 9152

Trigo, I. F., Monteiro, I. T., Olesen, F., Kabsch, E.: An assessment of remotely sensed land surface temperature. J. Geophys. Res., 113, D17108, doi:10.1029/2008JD010035, 2008. 9138

Trigo, I. F., DaCamara, C. C., Viterbo, P., Roujean, J.-L., Olesen, F., Barroso, C., Camacho-de Coca, F., Carrer, D., Freitas, S. C., Garcia-Haro, J., Geiger, B., Gellens-Meulenberghs, F., Ghilain, N., Melia, J., Pessanha, L., Siljamo, N., and Arboleda, A.: The Satellite Application Facility on Land Surface Analysis, Int. J. Remote Sens., 32, 2725–2744, doi:10.1080/01431161003743199, 2011. 9116

van den Hurk, B. J. J. M., Viterbo, P., Beljaars, A. C. M., and Betts, A. K.:. Offline validation of the ERA40 surface scheme, ECMWF Technical Memorandum No. 295, 41 pp, 2000. 9115, 9119, 9120, 9121

van den Hurk ,B. J. J. M., Viterbo P., and Los S.: Impact of leaf area index seasonality on the annual land surface evaporation in a global circulation model, J. Geophys. Res., 108, 4191, doi:10.1029/2002JD002846, 2003. 9115, 9127

Verger, A., Camacho, F., García-Haro, F. J., and Meliá, J.: Prototyping of Land-SAF leaf area index algorithm with VEGETATION and MODIS data over Europe, Remote Sens. Environ., 113, 2285–2297, doi:10.1016/j.rse.2009.06.009, 2009. 9119

Verhoef, A., McNaughton, K. G., and Jacobs, A. F. G.: A parameterization of momentum roughness length and displacement height for a wide range of canopy densities, Hydrol. Earth Syst. Sci., 1, 81–91, doi:10.5194/hess-1-81-1997, 1997. 9118

Viterbo, P. and Beljaars, A. C. M.: An improved land surface parameterization scheme in the ECMWF model and its validation, J. Climate, 8, 2716–2748, 1995. 9120

Williams, M., Richardson, A. D., Reichstein, M., Stoy, P. C., Peylin, P., Verbeeck, H., Carvalhais, N., Jung, M., Hollinger, D. Y., Kattge, J., Leuning, R., Luo, Y., Tomelleri, E., Trudinger, C. M., and Wang, Y.-P.: Improving land surface models with FLUXNET data, Biogeosciences, 6, 1341–1359, doi:10.5194/bg-6-1341-2009, 2009. 9130

HESSD
8, 9113–9171, 2011

Table 1. List of PFTs defined in ECOCLIMAP-I and used in the land surface model.

code	PFT
1	Bare Soil
2	Rocks
3	Snow (Permanent)
4	Deciduous Broad leaf Forest (DBF)
5	Evergreen Needle leaf Forest (ENF)
6	Evergreen Broad leaf Forest (EBF)
7	C3 crops
8	C4 crops
9	Irrigated crops
10	Grassland (G)
11	Swamp areas and bogs

HESSD
8, 9113–9171, 2011

Table 2. h_{veg} for each ECOCLIMAP-I PFT. h is tabulated in ECOCLIMAP-I database (Masson et al., 2006), and depends on the geographical location.

$h_{veg} = \min(1.0, \exp^{(LAI-3.5)/1.3})$	C3 crops
$h_{veg} = \min(2.5, \exp^{(LAI-3.5)/1.3})$	C4 crops
$h_{veg} = h$	trees
$h_{veg} = LAI/6$	grassland
$h_{veg} = 0.01$ m	bare soil and snow
$h_{veg} = 1.0$ m	rocks

HESSD
8, 9113–9171, 2011

Table 3. In-situ eddy covariance observations used in this study (Sites, years and references).

Site	Country	Years	Reference
Skukuza	S. Africa	2008–2009	Kutsch et al. (2008)
Vielsalm	Belgium	2007–2008	Aubinet et al. (2001)
Tojal	Portugal	2007	Pereira et al. (2007)
Puéchabon	France	2007	Joffre et al. (1996)
Agoufou	Mali	2007	Merbold et al. (2009)
Tchizalamou	R. Congo	2007	Merbold et al. (2009)
Wetzstein	Germany	2007	Rebmann et al. (2010)
Sodankylä	Finland	2007	Suni et al. (2003)
Demokeya	Sudan	2007–2009	Sjöström et al. (2009)

HESSD
8, 9113–9171, 2011

Table 4. Comparison of simulations with ECOCLIMAP-I (ECO) or LSA-SAF LAI (LSA) against 30 min observed LE ($W m^2$): statistical scores: correlation coefficient (ρ), root mean square error (RMSE), bias and NS (Nash and Suttcliffe, 1970). Improved NS with LSA compared to ECO are highlighted.

Station	Mode	ρ	RMSE	Bias	NS
Skukuza	ECO	0.754	85.07	−37.86	0.46
	LSA	0.787	73.25	−6.25	**0.60**
Demokeya	ECO	0.768	53.41	−18.55	0.53
	LSA	0.795	48.39	−5.26	**0.62**
Tchizalamou	ECO	0.760	60.14	3.16	0.51
	LSA	0.775	58.68	9.11	**0.53**
Agoufou	ECO	0.612	83.56	−32.40	0.26
	LSA	0.695	72.42	−18.37	**0.45**
Puéchabon	ECO	0.817	44.42	−9.29	0.61
	LSA	0.85	40.83	2.71	**0.67**
Tojal	ECO	0.849	41.98	−5.94	0.66
	LSA	0.828	45.37	−6.95	0.61
Vielsalm	ECO	0.747	46.89	10.88	0.47
	LSA	0.712	47.75	8.73	0.46
Wetzstein	ECO	0.832	53.14	−26.78	0.57
	LSA	0.850	48.83	−22.94	**0.64**
Sodankyla	ECO	0.711	29.59	−8.68	0.39
	LSA	0.735	28.16	−11.08	**0.44**

HESSD
8, 9113–9171, 2011

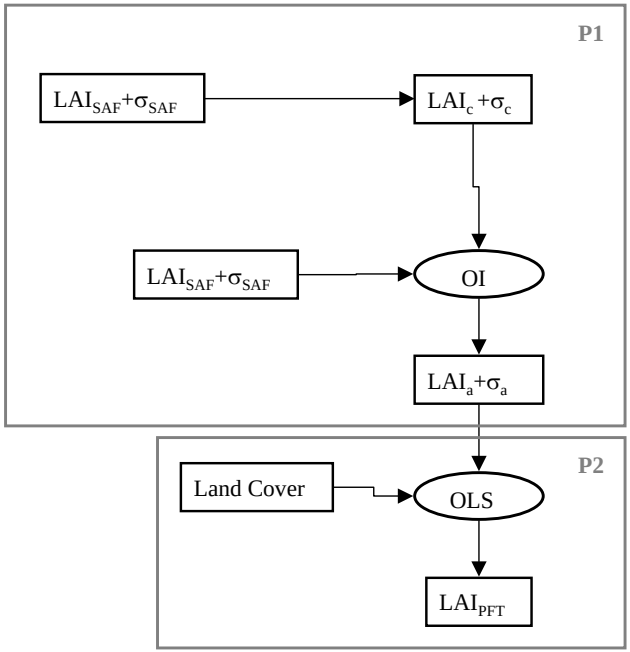

Fig. 1. Flowchart of the two-steps procedure to obtain LAI for each PFT in a given MSG/SEVIRI pixel. From P1, continuous and consistent LAI series are created at pixel level, LAI_a, using a 4-yr climatology from LSA-SAF LAI, LAI_{SAF}, actual LAI_{SAF}, and an optimal interpolation (OI) method. In P2, the pixel LAI is decomposed into LAI_{PFT} for each PFT contributing to the pixel area, using a land cover map, LAI_a and an ordinary least square method (OLS).

HESSD
8, 9113–9171, 2011

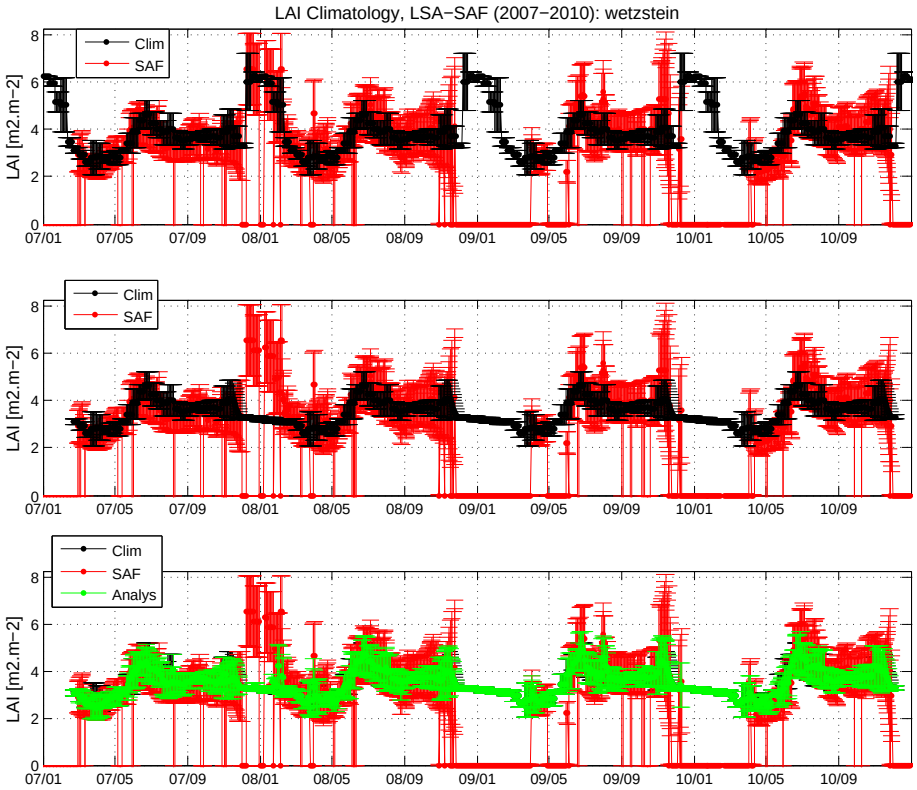

Fig. 2. Illustration of the pre-processing of LSA-SAF LAI images on a test case over a forest (Wetzstein) in Germany. **(a)** A 10-days composite (black) is derived from LSA-SAF LAI daily data (red). **(b)** Spurious data are filtered out, and linear interpolation is applied to create the climatology, LAI_c (black). **(c)** At last, an optimal interpolation scheme (OI) is applied using the climatology and the actual LSA-SAF LAI, LAI_{SAF}, to provide the analysed LAI, LAI_a.

HESSD
8, 9113–9171, 2011

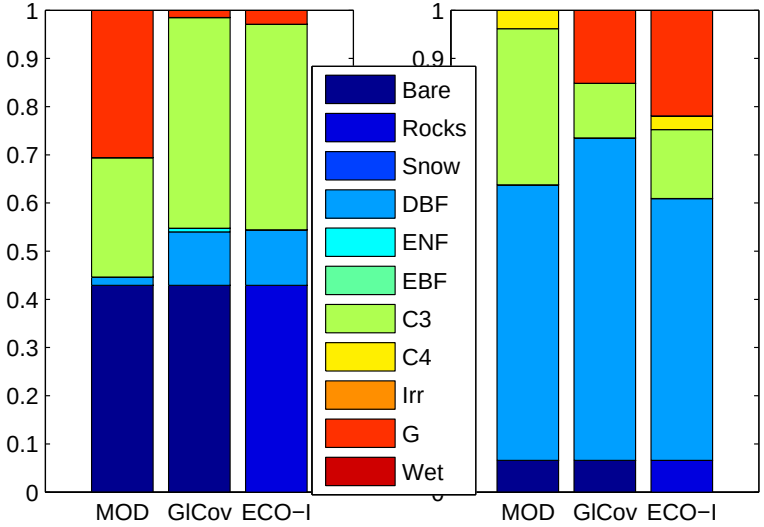

Fig. 3. Comparison of MODIS MCD12Q1 (2007), GlobCover v2.2 and ECOCLIMAP-I land covers for 2 MSG/SEVIRI pixels over Europe (in Portugal and France, respectively).

HESSD
8, 9113–9171, 2011

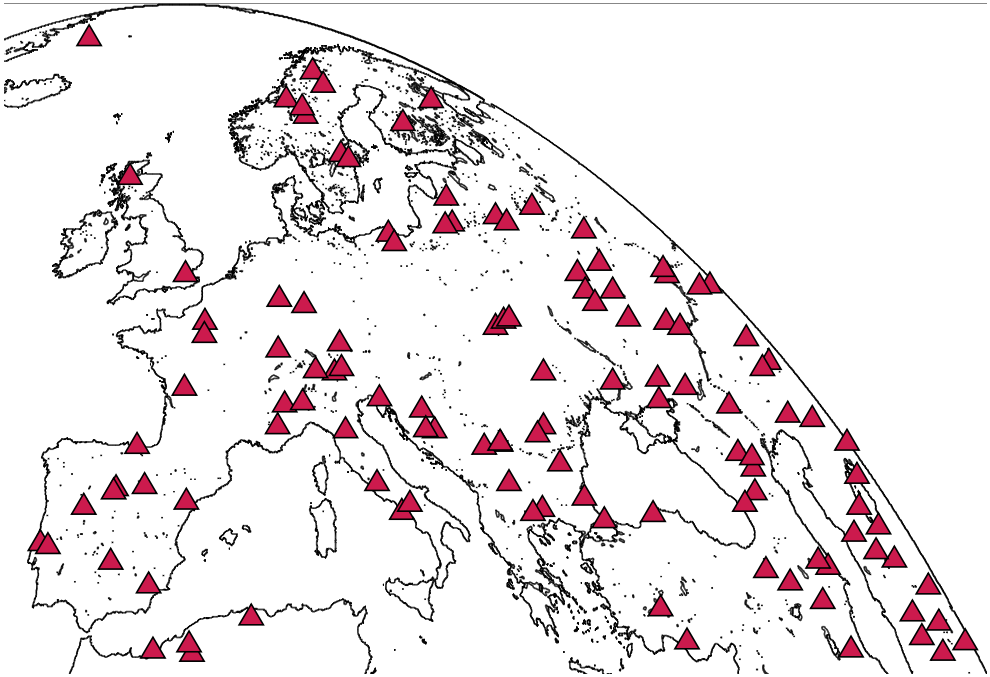

Fig. 4. Location, in the satellite projection over Europe, of 120 MSG/SEVIRI pixels selected randomly.

HESSD
8, 9113–9171, 2011

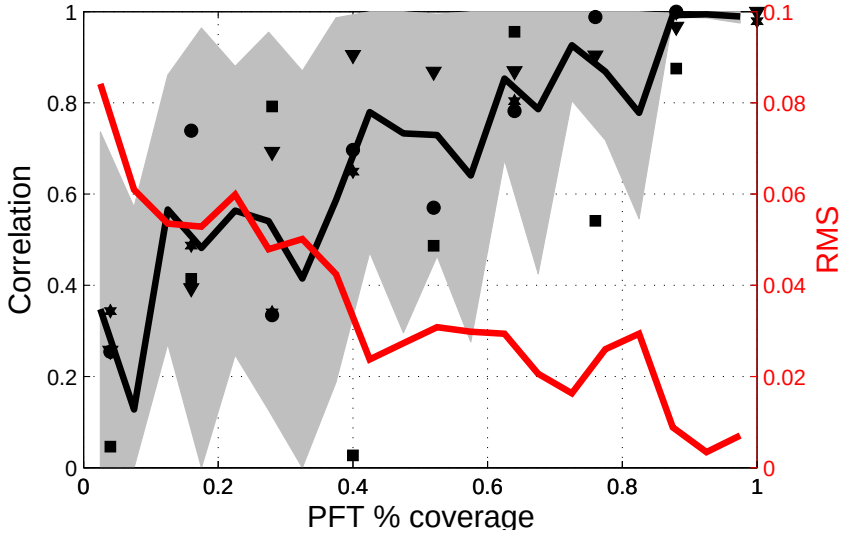

Fig. 5. Mean correlation (black line) between LAI time series obtained using ECOCLIMAP-I, GLOBCOVER and MODIS land covers, and its dependence in the PFT percentage in a given MSG/SEVIRI pixel. The grey shaded area represents the dispersion of the correlation. PFT dependent correlation is superimposed (DBF: ∘, ENF: □, Crops: ▽, Grass: ∗). In addition, RMS resulting from the comparison of the time series is shown in red.

HESSD
8, 9113–9171, 2011

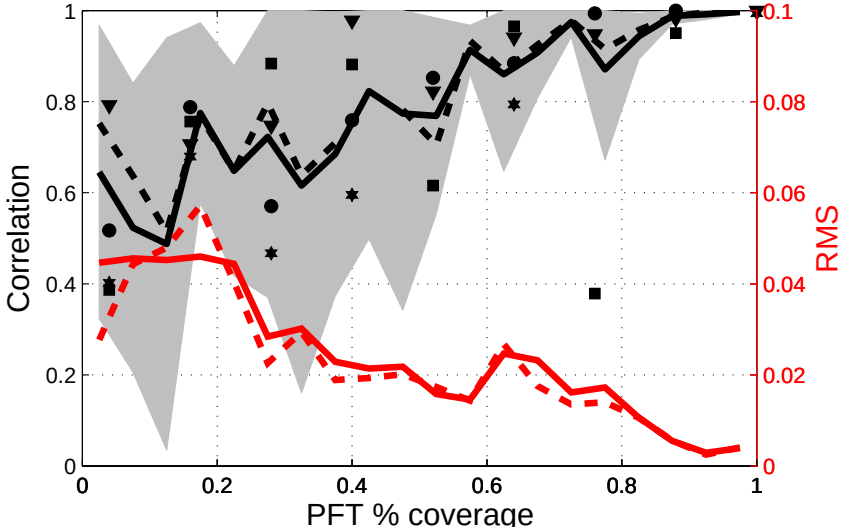

Fig. 6. Same as Fig. 5, but for a 5 × 5 (solid) and 7 × 7 (dashed) neighbourhood.

HESSD
8, 9113–9171, 2011

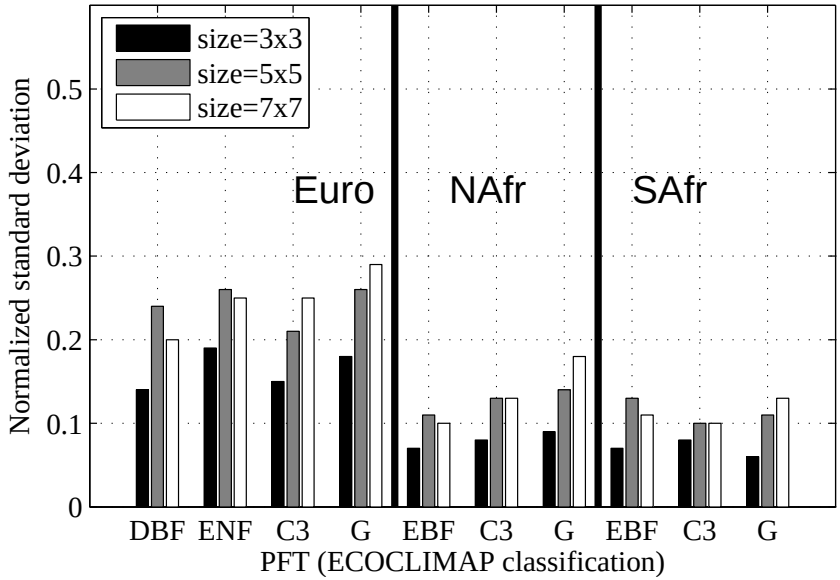

Fig. 7. Normalized PFT intra-variability (standard deviation) of LAI in function of the neighbourhood size for Europe (Euro) and Africa (NAfr and SAfr).

HESSD
8, 9113–9171, 2011

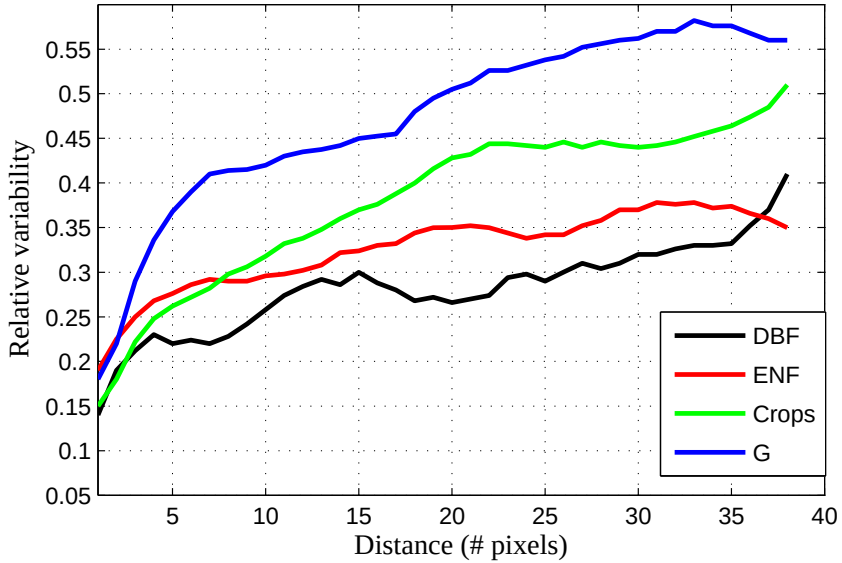

Fig. 8. Relative variability of LAI with Distance (# pixels) to nearest Hg pixel, by PFT, i.e. C3 crops (black), DBF (red), ENF (blue), G (green), in Europe.

HESSD
8, 9113–9171, 2011

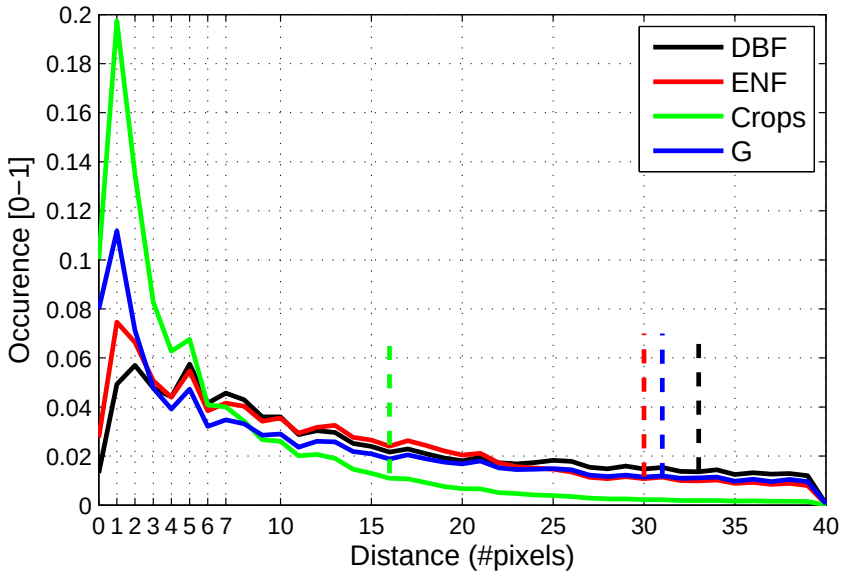

Fig. 9. Distance (# pixels) to nearest Hg pixel by PFT, i.e. C3 crops (black), DBF (red), ENF (blue), G (green), in Europe. Vertical dashed lines denote the 90 % of the cumulative distribution for each PFT.

HESSD
8, 9113–9171, 2011

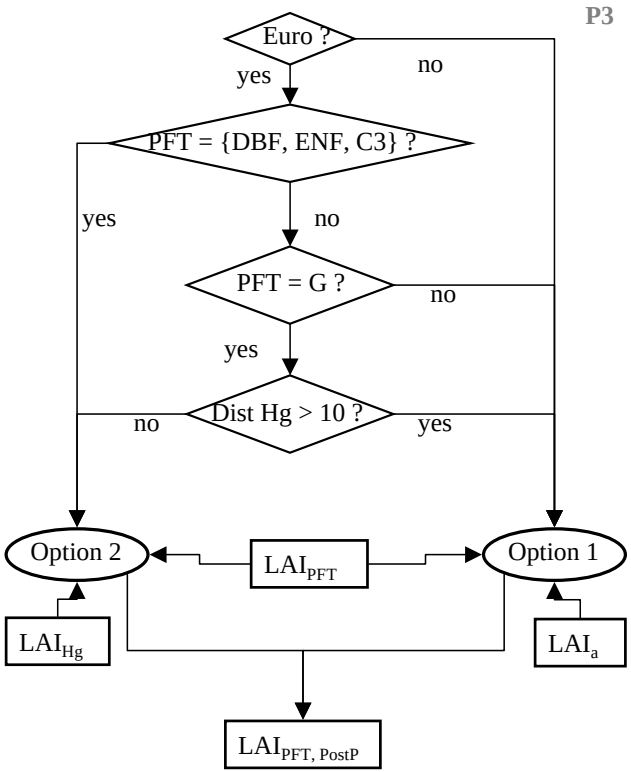

Fig. 10. Flowchart P3 with post-processing steps of PFT derived LSA-SAF LAI, LAI_{PFT}, to obtain a consistent LAI, $LAI_{PFT,PostP}$.

HESSD
8, 9113–9171, 2011

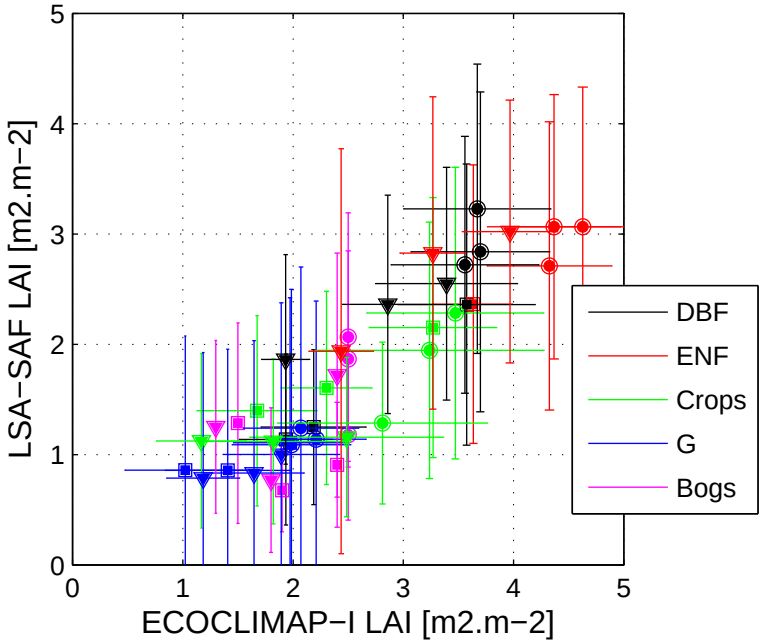

Fig. 11. Comparison of monthly mean and variability of LAI between ECOCLIMAP-I and LSA-SAF, for March to November 2007 over Europe. March to May (□), June to August (∘), September to November (▽).

HESSD
8, 9113–9171, 2011

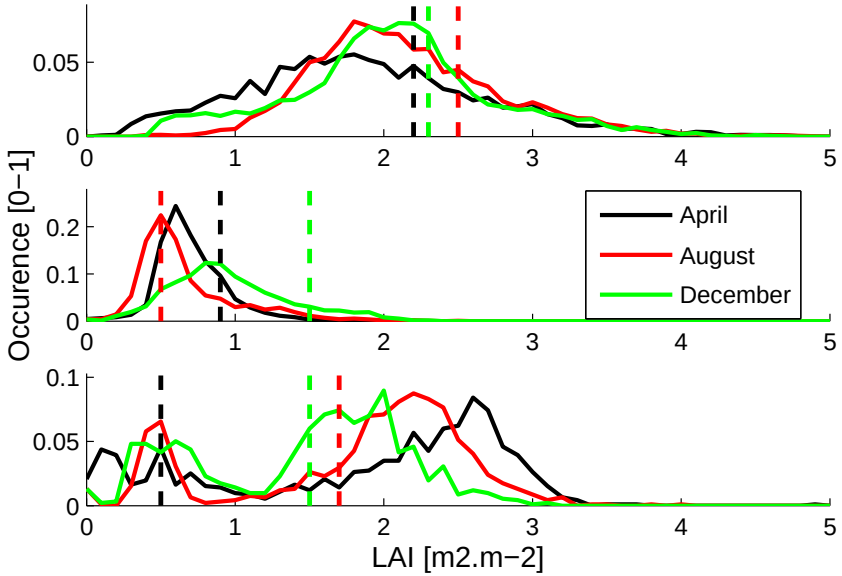

Fig. 12. Distribution of LSA-SAF LAI (continuous lines) against ECOCLIMAP-I monthly values (dashed vertical lines) for 3 dates (15 April, 15 August and 15 December 2007) for 3 homogeneous ecosystems: Tropical African Grassland (top), Semi-Arid African grassland (middle) and Nile Valley and desertic crops (bottom).

HESSD
8, 9113–9171, 2011

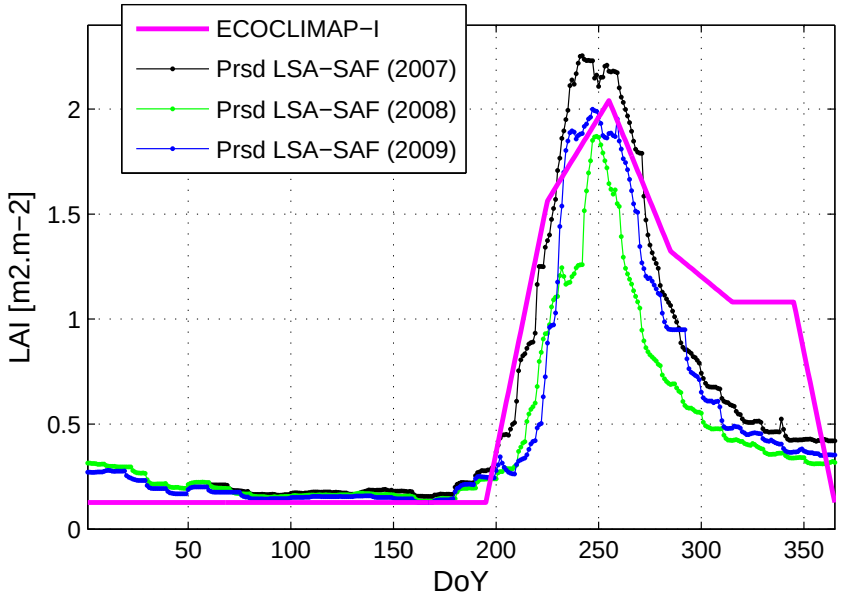

Fig. 13. Time series comparison of processed LSA-SAF LAI (Prsd LSA-SAF) for 2007, 2008 and 2009, and re-scaled and linearly interpolated ECOCLIMAP-I LAI for a pixel in Western Africa (15.29° N, 1.49° W).

HESSD
8, 9113–9171, 2011

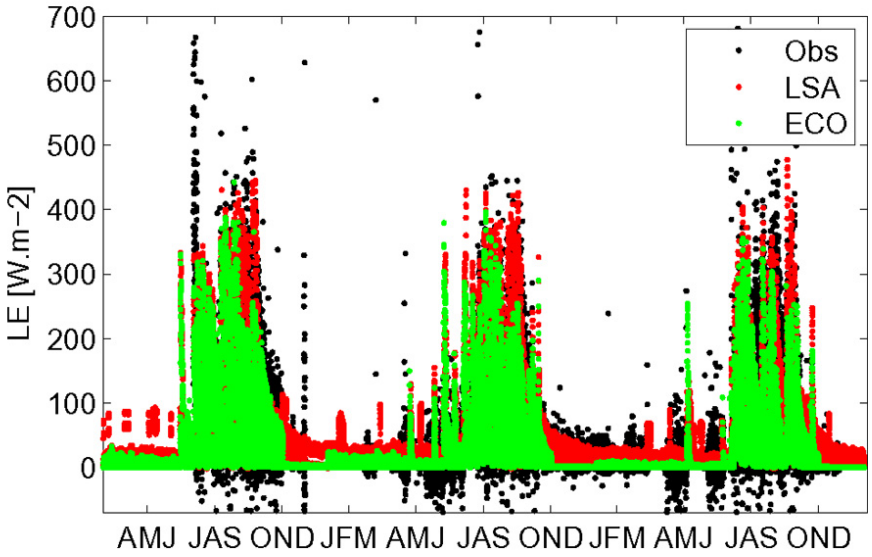

Fig. 14. Comparison of LE for Demokeya for 2007, 2008 and 2009; observed in (Obs: black), simulation using ECOCLIMAP-I (ECO: green), simulation using LSA-SAF LAI (LSA: red).

HESSD
8, 9113–9171, 2011

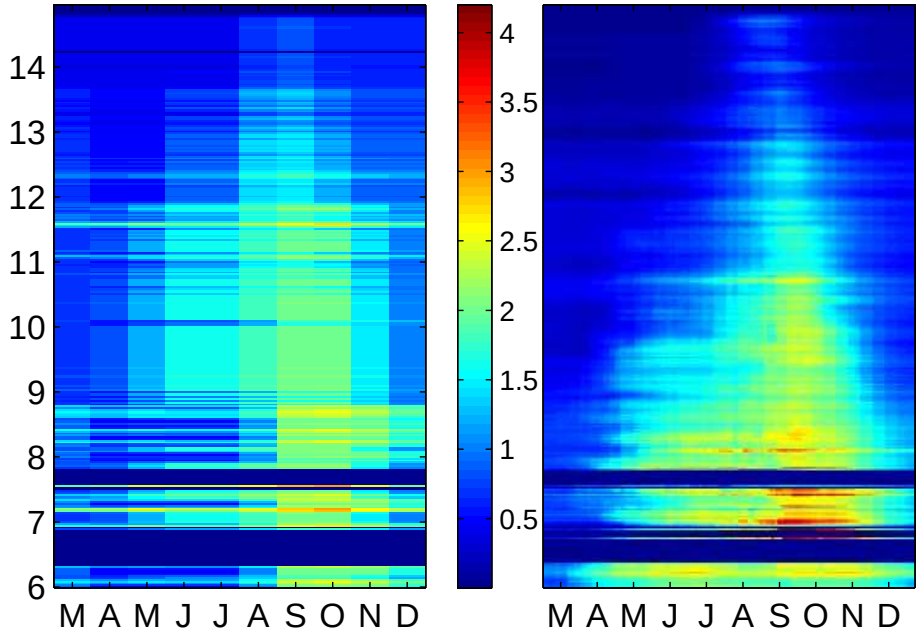

Fig. 15. LAI evolution (March to December 2007) over the transect: ECOCLIMAP-I (left) and LSA-SAF LAI (right).

HESSD
8, 9113–9171, 2011

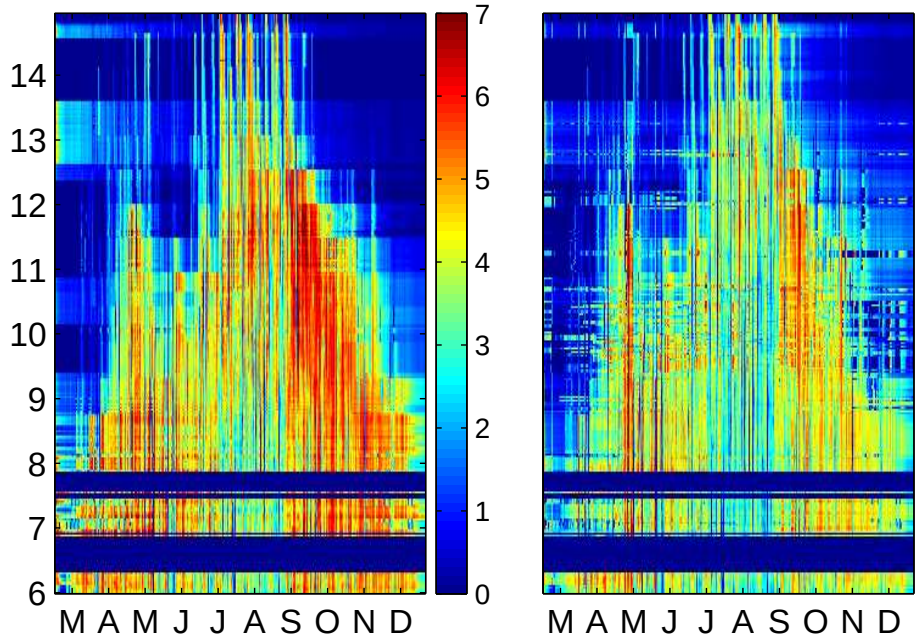

Fig. 16. Simulations along the North-South transect in West Africa from 15° N to 6° N: daily ET [mm] simulated using ECOCLIMAP-I (left) and LSA-SAF LAI (right).

HESSD
8, 9113–9171, 2011

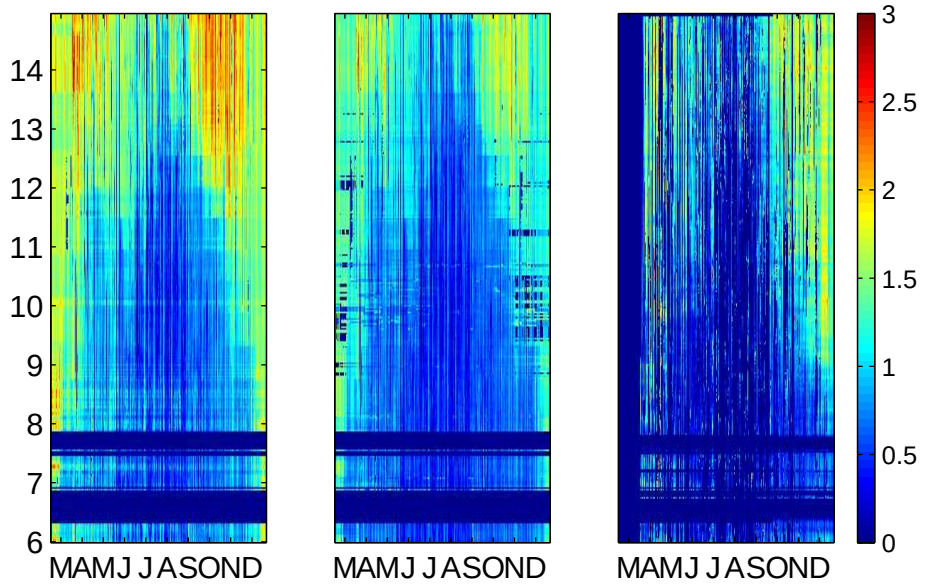

Fig. 17. Daily morning surface heating rates [$K\,h^{-1}$] for a transect in West Africa from 15° N to 6° N: simulation using ECOCLIMAP-I (left) or LSA-SAF LAI (middle), obtained from LSA-SAF LST (right).

HESSD
8, 9113–9171, 2011

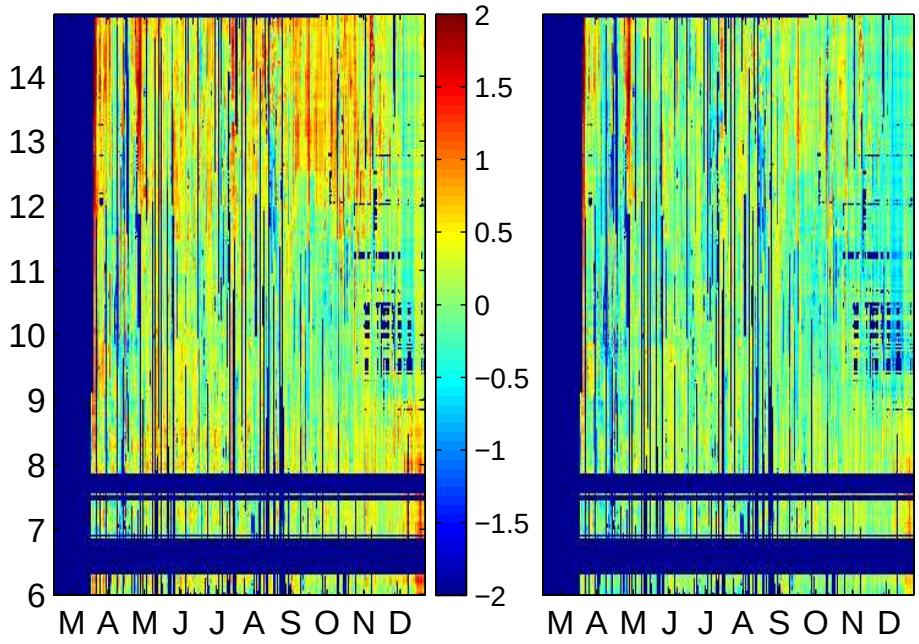

Fig. 18. Differences in the daily morning surface heating rates [$K\,h^{-1}$] (same transect Fig. 17): simulated heating rates using ECOCLIMAP-I vs. LSA-SAF LST(left), simulated heating rates using LSA-SAF LAI vs LSA-SAF LST (right).

HESSD
8, 9113–9171, 2011